TURUN YLIOPISTO

RAB24 interaction between GOLGA3, USO1 and emerin

Johannes Tapio

Physiology and genetics
Master's thesis
Credits: 30

12.11.2024
Turku

Master's thesis

Subject: Physiology and genetics
Author: Johannes Tapio
Supervisors: Lav Tripathi and Eeva-Liisa Eskelinen
Number of pages: 48 pages + 5 appendix pages
Date: 12.11.2024

RAB proteins are small GTPases responsible for controlling membrane trafficking in eukaryotic cells. RAB24 is a unique RAB protein, due to its low GTPase activity. It is implicated to function at later stages of basal autophagy and in the endocytic degradation pathway. It is also required for normal cell division and plays a role in liver cell homeostasis. A point mutation in RAB24 causes hereditary ataxia in dogs, potentially through disruptions in the autophagic process. In addition, increased expression of RAB24 promotes a malignant phenotype of hepatocellular carcinoma (HCC) cells.

The exact functional mechanisms of RAB24 are still unknown. Critical in this regard is to identify the proteins that RAB24 interacts with in the cell. Using proximity labeling, the Eskelinen group discovered new putative RAB24 interaction partners, of which three are studied in this thesis; Golgin subfamily A member 3 (GOLGA3), General vesicular transport factor p115 (USO1, also called VDP) and emerin.

The aim of this thesis was to investigate whether GOLGA3, USO1 and emerin physically interact with RAB24, and whether they co-localize with RAB24 within the cell. We used co-immunoprecipitation (co-IP) to study the physical interaction between the proteins, and immunofluorescence microscopy to visualize and quantify protein co-localization. Experiments were conducted using the human liver cancer-derived cell lines Hep G2 and Huh-7. Interaction between RAB24 and the three candidate proteins could not be confirmed, as the co-IP results were inconsistent. USO1 was found to partially co-localize with RAB24.

Key words: RAB24, RAB, GOLGA3, USO1, emerin, autophagy

Table of contents

1 Introduction

1.1 Membrane trafficking and RAB proteins

Eukaryotic cells are divided into multiple different compartments with unique functions, separated by lipid bilayer membranes. These membranes are highly dynamic, which is essential for the process of membrane trafficking. Membrane trafficking forms a network inside the cell, through which the different cellular compartments communicate and coordinate their functions. It is a process where membrane vesicles containing cargo, such as neurotransmitters, hormones or plasma membrane receptors bud off from donor compartments and are transported to their specific destinations, either inside the cell or to the plasma membrane. The transportation of these vesicles is organized through directional routes that can be roughly divided into the exocytic and endocytic pathways. The exocytic pathway leads outward from the endoplasmic reticulum (ER) to the Golgi apparatus, from where the transport continues to several different destinations inside the cell, or all the way to the cell surface. Conversely, the endocytic pathway flows inward from the plasma membrane, delivering extracellular substances or plasma membrane components inside the cell in endocytic vesicles. From there, they may be returned to the plasma membrane, translocated to another side of the cell via the transcytotic pathway or sent to lysosomes for breakdown and reuse (Alfonso et al., 2009). Each step in membrane traffic has a return pathway to the opposite direction. This ensures the maintenance of the size and composition of the membrane-bound organelles.

Membrane trafficking is tightly regulated at every step, from selecting cargo and forming vesicles to their transport, tethering, and fusion, ensuring that cargo reaches the correct destination. The diverse group of small GTPases are responsible for regulating membrane trafficking processes. To do this, each small GTPase specifically localizes to the membranes where it operates. Small GTPases switch between a GTP-bound active form and a GDP-bound inactive form. The nucleotide transition causes a change in the conformation of the GTPase, which promotes the activation or deactivation of effector molecules, such as vesicle tethers, motor proteins, kinases, or various adaptor proteins (Stenmark, 2009). GTPase Activating Proteins (GAPs) promote the hydrolysis of GTP to

GDP, while Guanine Exchange Factors (GEFs) facilitate the transition from GDP to GTP (Johnson & Chen, 2012).

Most small GTPases are part of the extensive RAS superfamily, which includes over 150 identified members. This superfamily is categorized into five families with overlapping functions: RAS, ARF/SAR, RHO, RAN and RAB GTPases (Song et al., 2019). With over 60 members in humans, the RAB GTPases form the largest subfamily. They are involved in various membrane trafficking processes (Stenmark, 2009). RAB GTPases attach to their target membranes through hydrophobic geranylgeranyl groups that are post-translationally added to their C-terminal cysteines (Pereira-Leal et al., 2001)

Like other small GTPases, RAB GTPases cycle between a GTP-bound active form and a GDP-bound inactive form (Figure 1). Most effectors engage with the GTP-bound form of RAB proteins, although effectors binding to GDP-bound RABs have also been reported (Shirane & Nakayama, 2006). The structural variation between the active GTP-bound and the inactive GDP-bound forms of RABs are subtle, primarily occurring in the Switch-1 and Switch-2 regions. Upon transition from GDP-bound to GTP-bound form or vice-versa, conformational changes in these two switch regions regulate the interaction with effectors and the following membrane trafficking steps. Generally, in the GTP-bound form, Switch-I and Switch-II appear to have a well-defined structure, making them easily accessible to their specific downstream cellular partners (Pylypenko et al., 2018; Vetter & Wittinghofer, 2001).

RABs have intrinsically slow GTPase and nucleotide exchange characteristics, which are stimulated by GAPs and GEFs, respectively. Other RAB regulatory proteins include GDP-dissociation inhibitors (GDIs) and RAB escort proteins (REPs). GDIs prevent the dissociation of GDP from RABs (Matsui et al., 1990) and increase the cytoplasmic pool and recycling of RAB proteins (Wilson et al., 1996) . REPs are a part of multisubunit enzymes known as RAB geranylgeranyl transferases (RAB-GGTases) and help in the recruitment of newly synthesized RABs to the catalytic component of the enzyme, where the RABs are geranylgeranylated from their C-terminus. Later, they escort the geranylgeranylated RABs to their specific membranes (Goody et al., 2005). GDI-displacement factor (GDF) is another reported RAB regulatory protein which acts to dissociate endosomal RABs from GDIs (Dirac-Svejstrup et al., 1997). However, a recent

study indicated that GDF is thermodynamically unnecessary and GDP-GTP exchange by GEF is sufficient to stabilize the GDI-dissociated form of RAB (Schoebel et al., 2009).

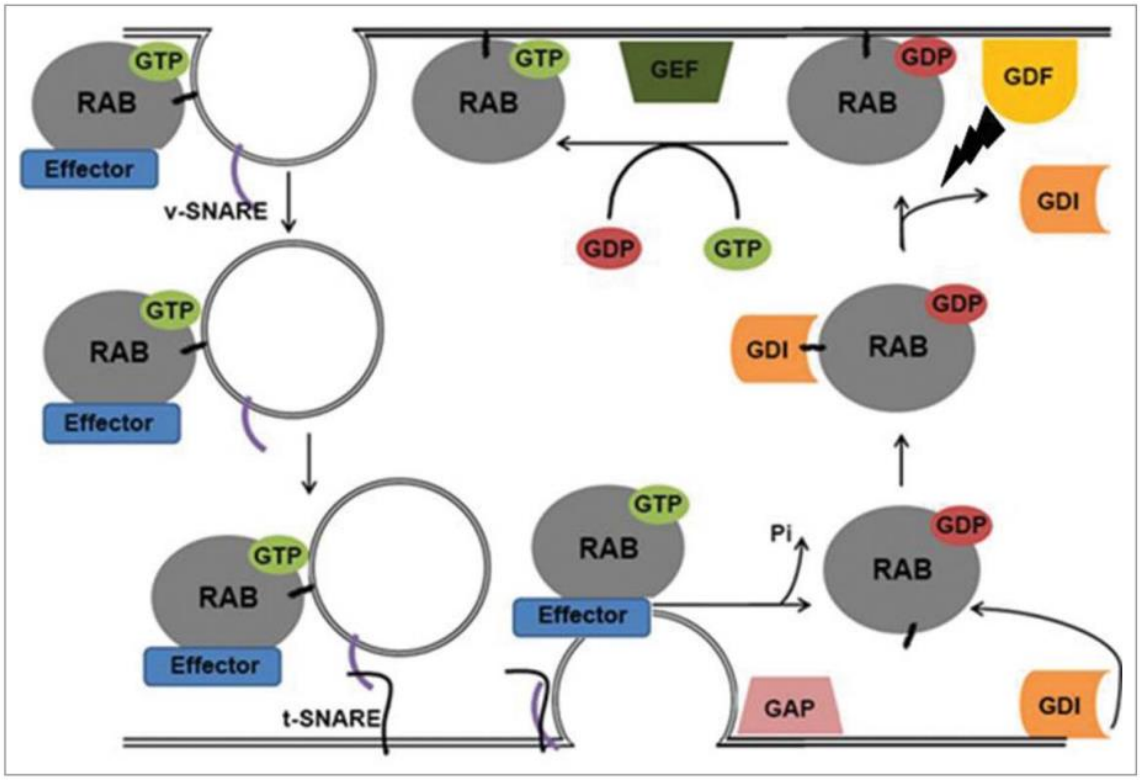

Figure 1. RAB GTPase cycle. A guanine-nucleotide-exchange factor (GEF) replaces GDP bound to a RAB GTPase with GTP, causing a conformational change that allows specific effector proteins to recognize and interact with the RAB. These effector proteins help deliver the vesicle and its cargo to a specific destination. SNARE proteins (v-SNARE and t-SNARE) in the vesicle and target membranes mediate vesicle fusion. A GTPase-activating protein (GAP) enhances the GTPase activity of the RAB, leading to the hydrolysis of GTP to GDP and the release of an inorganic phosphate (Pi). A GDP dissociation inhibitor (GDI) facilitates the release of the RAB from the membrane and solubilizes it in the cytosol. A GDI displacement factor (GDF) then dissociates GDI from the RAB, allowing the RAB to reattach to the membrane. Picture from (Ylä-Anttila & Eskelinen, 2018).

1.2 RAB24 is a unique RAB protein

RAB24 is characterised as one of the primordial RAB proteins, found in the last common ancestor of all eukaryotes (Elias et al., 2012). It is conserved in many species, such as in mammals and zebrafish, but lost in others like *Drosophila melanogaster* and *Caenorhabditis elegans*. Olkkonen et al. first discovered RAB24 as localizing to the ER/*cis*-Golgi region and late endosomal structures. They found RAB24 to be expressed in various tissues throughout the body, with the highest levels found in the brain (Olkkonen et al., 1993). Later, RAB24 was also found to localize in autophagic vacuoles (Ylä-Anttila et al., 2015).

Erdman et al. reported many unusual features of RAB24 contrasted to other RAB proteins (Erdman et al., 2000). Firstly, they found that RAB24 is primarily found in the GTP-bound state, indicating that it has a low GTPase activity. This could be related to the presence of an unusual serine at position 67 in the nucleotide-binding region of RAB24. The corresponding amino acid in other RAB proteins is glutamine, and when Erdman et al. performed site-directed mutagenesis to replace the serine with glutamine, RAB24 was found mostly in the GDP-bound form, indicating increased GTPase activity. Interestingly, when the glutamine in other RAB proteins is replaced with a leucine, the mutation leads to a constitutively active, GTP-bound phenotype, whereas RAB24-S67L has reduced GTP binding. In addition, RAB24-S67L does not localize to any specific membranes but is cytoplasmic (Ylä-Anttila et al., 2015). Erdman et al. also found a difference in the NKxD motif of RAB24. The NKxD motif interacts with the guanine of GTP/GDP and is one of the five conserved motifs of the GTP-binding region of small GTPases (Rensland et al., 1995; Yin et al., 2023). The NKxD motif of RAB24 is unique among RAB proteins, as the motif has a substitution of asparagine in place of threonine (Thr-120) (Erdman et al., 2000). Besides RAB24, the threonine variation is found only in the functionally distinct CDC42/RAC family of GTPases. (Valencia et al., 1991; Valencia & Sander, 1995).

Erdman et al. also found that compared to RAB1, RAB24 was insufficiently geranylgeranylated and mostly localized in the cytosol—not associated with membranes (Erdman et al., 2000). They discovered that the C-terminal cysteine residues that undergo geranylgeranylation in RAB proteins are uniquely organized in RAB24; the RAB24 C-

terminal has a CCXX motif with two histidine residues in the terminal XX positions (CCHH). A CCXX motif occurs also in RAB5 and RAB17, but the two terminal histidine residues are found only in RAB24. However, they discovered that this was not the only cause for the insufficient geranylgeranylation, and that other unidentified features were involved. However, later studies showed that RAB24 geranylgeranylation was comparable to RAB7, and necessary for its localization to autophagic vacuoles (Ylä-Anttila et al., 2015).

Lastly, Ding et al. provided evidence for tyrosine phosphorylation of RAB24. Cytosolic RAB24 was phosphorylated more compared to membrane-bound RAB24 (Ding et al., 2003). They found two phosphorylated tyrosines: Y172 in the YXXφ motif and Y17 in the conserved P-loop motif. The YXXφ motif is located in the hypervariable domain, which comprises the last 30 or more amino acid residues at the C-terminus of RAB proteins. The domain exhibits high sequence variation among RABs and is suggested to be crucial for their specific subcellular targeting (Chavrier et al., 1991). Interestingly, the second phosphorylated tyrosine in RAB24 is located in the P-loop, which is involved in GTP hydrolysis (Zhu et al., 2003). This could contribute to the reduced GTPase activity of RAB24.

1.3 Functions of RAB24

While the exact molecular mechanisms of RAB24 remain unknown, there has been progress in the research of its functions. Notably, RAB24 has been found to partake in the regulation of the autophagic pathway (Ylä-Anttila et al., 2015). Autophagy is an evolutionarily conserved process in eukaryotic cells, where the cell degrades its own cytoplasmic components using the lysosomal machinery. Autophagy helps maintain cellular homeostasis by providing metabolites for energy production and biosynthetic processes when the cell is undergoing starvation (Yorimitsu & Klionsky, 2005). Autophagy also aids in cellular maintenance by degrading unnecessary or impaired organelles and misfolded or aggregated proteins (Yang & Klionsky, 2010). In addition, it can degrade invading intracellular pathogens (Levine & Kroemer, 2008). In macroautophagy—generally referred to as autophagy—the cytoplasmic cargo is enclosed within a vesicle with two limiting lipid bilayers, called an autophagosome.

Autophagosomes subsequently merge with late endosomes to form amphisomes, which then merge with lysosomes to create autolysosomes, where the contents are broken down. (Parzych & Klionsky, 2014).

Autophagy can be induced during nutrient starvation or cellular damage as a stress response, but there is also a form of autophagy that is constantly active, namely basal autophagy. Basal autophagy is responsible for cellular housekeeping by degrading protein aggregates and damaged organelles. Basal autophagy and starvation-induced autophagy differ in their regulation and substrate selectivity. The target of rapamycin (mTOR) kinase represses starvation-induced autophagy but affects basal autophagy to a lesser degree (Yamamoto et al., 2006). However, Musiwaro et al. demonstrated that overexpression of RHEB and RAG—two mTOR activators—did inhibit basal autophagy (Musiwaro et al., 2013).

RAB7 is required for the final maturation of starvation-induced autophagosomes (Jäger et al., 2004). RAB24, on the other hand, seems to be required for the final stages of basal autophagy, as Ylä-Anttila et al. demonstrated that during basal conditions, depletion of RAB24 led to the accumulation of acidic autolysosomes. RAB24 was not necessary for the formation, maturation and clearance of autophagosomes induced by starvation (Ylä-Anttila et al., 2015). Currently, two pathways for autolysosome clearance are known. In lysosomal exocytosis, autolysosomes fuse with the plasma membrane. In the autophagic lysosome reformation (ALR) pathway lysosomes reform from autolysosomes (Y. Chen & Li, 2012; Settembre et al., 2013). Whether RAB24 plays a role in the regulation of these pathways remains to be seen.

RAB24 expression increases in response to cellular stress, potentially due to increased autophagy as a response to the stress. Egami et al. found increased mRNA levels of RAB24 in nerve-injured hypoglossal motor neurons (Egami et al., 2005). They also reported the induction of microtubule-associated protein light chain 3 (LC3) mRNA and accumulation of LC3-II—common markers used for measuring autophagic flux—as a result of nerve cell injury, suggesting an increased autophagic activity in these cells. They also reported increased RAB24 mRNA and LC3 mRNA levels and accumulation of LC3-II following proteasome inhibitor treatment (MG132) in differentiated PC12 cells, further suggesting that the increased RAB24 expression levels were a response to enhance the

degradation of unused and misfolded proteins. In addition, Seki et al. reported similar results in the trigeminal motor nucleus of rats, where RAB24 protein levels were increased after denervation (Seki et al., 2009).

RAB24 has been implicated in another degradation pathway besides autophagy, namely the late endosome/lysosome pathway (Amaya et al., 2016). This degradation pathway begins with endocytosed cargo localizing to vesicles called early endosomes. The early endosomes act as sorting stations, recycling some cargo back to the plasma membrane while directing others along the degradation pathway. In this pathway, early endosomes mature into late endosomes, which then merge with lysosomes to degrade the cargo. As discussed earlier, the endocytic degradation pathway intersects with the autophagic pathway through the formation of amphisomes, when autophagosomes and late endosomes fuse together. The two pathways also share common regulatory proteins, such as RAB7. RAB7 is a necessary component in the final stage of both late endosome and late autophagosome maturation, where they fuse with lysosomes (Hyttinen et al., 2013; Jäger et al., 2004). Amaya et al. demonstrated that RAB24 participates in the late endosome maturation, as it physically interacts and co-localizes with RAB7, and is needed for endocytic cargo degradation (Amaya et al., 2016). The proper localization of RAB7 to vesicular structures also depends on RAB24, as overexpression or knockdown of dominant negative RAB24 caused RAB7 to distribute in the cytosol. In addition, RAB24 was found to interact physically with the RAB7 effector protein RILP (RAB7 interacting lysosomal protein). This led the authors to hypothesize that RAB24 forms a complex on late endosomal/lysosomal compartments with RAB7 and RILP.

RAB24 has also been implicated in cell division. Militello et al. observed that distribution of RAB24 changed during the mitotic cell cycle (Militello et al., 2013). During interphase, RAB24 displayed a diffuse, perinuclear localization. However, during the mitotic phase, RAB24 was redistributed to localize in the mitotic spindle during metaphase, to the midbody during telophase and to the cleavage furrow during cytokinesis. Interestingly, RAB24 co-localized with microtubules during all these stages, and microtubule sedimentation assay showed that RAB24 co-sedimented with microtubules, indicating an association between RAB24 and microtubules. Militello et al. also found that transient overexpression of Myc-RAB24 in HeLa cells led to the formation of abnormal chromosome bridges connecting the two daughter cells after cytokinesis. Also, in CHO

cells stably transfected with GFP-RAB24, several abnormalities were found, such as binucleated and multinucleated cells, extremely large cells, abnormal spindle formation during metaphase, delayed movement of the chromosomes during telophase and multiple cytokinesis. RAB24 knockdown in HeLa cells also resulted in chromosome misalignment and abnormal spindle formation during metaphase, delayed movement of the chromosomes during telophase and cytokinesis failures.

Qiu et al. investigated the role of RAB24 in mouse oocyte meiosis (Qiu et al., 2019). During prophase RAB24 was diffuse but accumulated around the nucleus. During pre-metaphase RAB24 accumulated around the chromosomes, and during metaphase localized to the spindle region. RAB24 knockdown resulted in significant retardation of meiotic progression. Also, a high percentage of RAB24 knockdown oocytes displayed atypical spindles, chromosome misalignment, longer spindle lengths and a higher number of lagging chromosomes compared to control cells. RAB24 knockdown disrupted the kinetochore-microtubule interaction—which is crucial for proper attachment between the spindle and the chromosomes—as abnormal attachment was significantly more prevalent in RAB24 knockdown oocytes. RAB24 knockdown oocytes also exhibited a greater number of aneuploid eggs.

Taken together, the studies of Militello et al. (2013) and Qiu et al. (2019) suggest that RAB24 plays a role in the regulation of the cell division apparatus, possibly through association with microtubules.

Another potential function for RAB24 was discovered by Seitz et al., as they observed that RAB24 levels impacted several parameters of energy homeostasis in hepatocytes, possibly through regulating mitochondrial dynamics (Seitz et al., 2019). Firstly, they demonstrated that hepatic RAB24 knockdown in mice improved hepatic glucose tolerance, reduced apolipoprotein B (Apo B) levels, as well as serum total and low-density lipoprotein (LDL) cholesterol levels. Improvement in glucose tolerance was dependent on fibroblast growth factor 21 (FGF21), as FGF21 homozygous knockout inhibited the RAB24 knockdown effects. They also showed that RAB24 knockdown ameliorated liver steatosis and inflammation in mice fed with the methionine-choline-deficient high-fat diet (MCD-HFD), and reduced Nonalcoholic Steatohepatitis (NASH) markers, demonstrating a favorable effect of hepatic RAB24 knockdown in NASH development. Secondly, they

discovered that RAB24 knockdown increased mitochondrial respiration and ATP production, with mitochondria becoming more elongated and interconnected. Similar morphological changes occur during starvation-induced autophagy, where mitochondria elongate by fusing together, thus avoiding autophagic degradation and maintaining ATP production. Conversely, blocking elongation pharmacologically or genetically causes mitochondria to consume ATP, leading to starvation-induced cell death (Gomes et al., 2011). Seitz et al. demonstrated that RAB24 interacts with FIS1, a component of the mitochondrial fission complex. As the fission complex forms, it recruits dynamin-related protein 1 (DRP1) to the mitochondrial membrane, which in turn induces mitochondrial fission (Smirnova et al., 2001). RAB24 knockdown resulted in inefficient DRP1 recruitment to mitochondrial membranes and thus reduced mitochondrial fission, suggesting that the increased mitochondrial activity after RAB24 knockdown was due to its role as a regulator of mitochondrial dynamics via interaction with FIS1 (Seitz et al., 2019).

RAB24 has also been associated with diseases. Chen et al. investigated the dysregulation of the small regulatory RNAs, known as microRNAs (miRNAs), in hepatocellular carcinoma (HCC) and found that miR-615-5p expression was significantly attenuated in HCC (Chen et al., 2017). Interestingly, miR-615-5p was found to downregulate RAB24. The downregulation of miR-615-5p in HCC cells resulted in increased RAB24 expression. In cell cultures, RAB24 overexpression facilitated HCC cell growth and metastasis, thus implicating RAB24 as a promoter of the invasive phenotype of HCC cells. These findings align with the evidence showing that RAB24 plays a role in cell division, as discussed above (Militello et al., 2013; Qiu et al., 2019). Of note, Nonalcoholic fatty liver disease (NAFLD), and in particular its specific stage NASH, play a role in the formation of HCC. NASH is now the fastest-growing cause of HCC in Europe, South-East Asia and the United States (Llovet et al., 2021). As discussed above, RAB24 knockdown was found to ameliorate the symptoms of steatosis and inflammation in NASH (Seitz et al., 2019). Whether there is a connection in the molecular mechanisms of NASH and HCC in terms of RAB24 expression levels remains to be seen.

Agler et al. identified a point mutation in RAB24 in Gordon Setters and Old English Sheepdogs with hereditary ataxia (Agler et al., 2014). Hereditary ataxias constitute a varied class of hereditary neurodegenerative diseases, characterised by the degeneration

of the cerebellar cortex, particularly the Purkinje neurons, leading to muscle coordination dysfunctions (Hersheson et al., 2012; Seidel et al., 2012). The observed mutation in RAB24 leads to the replacement of glutamine with proline at position 38 of the amino acid sequence, within the putative Switch I region of RAB24 (Agler et al., 2014). Glutamine 38 is highly conserved in RAB24 across species, and its location in the functional Switch I region suggests that the Q38P mutation might affect nucleotide or effector binding (Gabe Lee et al., 2009; Eathiraj et al., 2005). RAB24-Q38P mutation resulted in the accumulation of ubiquitin-positive bodies in Purkinje neurons at the juncture of the granular and molecular layers, as well as in cells of the granular layer of the cerebellum. Accumulation of ubiquitin-positive bodies suggests a defect in the clearance of aggregated proteins within the neuronal cells. Interestingly, the accumulation of autophagic compartments in Purkinje cells was observed using electron microscopy, in line with the results implicating RAB24 as a necessary component in the clearance of late autophagic compartments (Ylä-Anttila et al., 2015).

1.4 RAB24 molecular mechanisms

Although there has been progress in the understanding of RAB24 functions, there are still many unanswered questions. Importantly, RAB24 effector proteins are unknown, although a few proteins have been shown to interact with RAB24. Several of these putative interacting proteins participate in membrane fusion events, consistent with studies linking RAB24 to autophagic and endocytic degradation pathways (Ylä-Anttila et al., 2015; Amaya et al., 2016). As discussed above, RAB24 was shown to co-precipitate with RAB7 and its effector RILP, known to be involved in the fusion process of endosomes and lysosomes (Amaya et al., 2016). Eskelinen group discovered that RAB24 co-precipitates with Vacuolar protein sorting-associated protein 18 (VPS18) and VPS41, members of the homotypic fusion and protein sorting (HOPS) tethering complex (Kotiniitty, 2024, and unpublished results). HOPS is a RAB7 effector complex and facilitates the fusion of late endosomal vesicles and autophagosomes with lysosomes (Balderhaar & Ungermann, 2013).

Schardt et al. observed co-precipitation between RAB24 and synaptosomal-associated protein 29 (SNAP-29) (Schardt et al., 2009). SNAPs are important components of the

SNARE complex, which mediates membrane fusion. The SNARE complex consists of a 4-helix bundle of SNARE proteins, each containing an individual SNARE domain, termed Qa-, Qb-, Qc- and R-SNARE. R-SNAREs (a VAMP protein, or v-SNARE) are usually incorporated into the membrane of a transport vesicle, whereas Qa-SNAREs (a syntaxin, or t-SNARE) are in the target membrane. They are then complexed together via Qb- and Qc-SNAREs. The Qb- and Qc-domains can be provided by the SNAP protein family, including SNAP-29. Together the SNAREs zipper into a tight complex and bring opposing membranes into contact, providing the energy necessary to fuse two lipid membranes together (Hong, 2005). The interaction of RAB24 with SNAP-29 was GTP independent, contrary to the interaction between RAB3A and SNAP-29, which was GTP dependent (Schardt et al., 2009). Interaction between SNAP-29 and various syntaxins has been observed (Steegmaier et al., 1998). Interestingly, SNAP-29 was found to interact with Syntaxin17 (STX17) and VAMP8, and together they were required for autophagosome-lysosome fusion (Itakura & Mizushima, 2013). SNAP-29 is necessary for both starvation-induced and basal autophagy, unlike RAB24. Also, whereas SNAP-29 and STX17 depletion led to the accumulation of double-membrane autophagosomes, RAB24 depletion resulted in the accumulation of acidic and degradative autophagic vacuoles bound by a single lipid bilayer membrane (Ylä-Anttila et al., 2015; Takáts et al., 2013; Itakura et al., 2012).

Behrends et al. performed a proteomic analysis of the autophagic interaction network (Behrends et al., 2010). The initial results of their mass spectrometry found HA-tagged RAB24 to co-precipitate with plakophilin 1, N-ethylmaleimide sensitive fusion protein (NSF) and GDP dissociation inhibitors 1 and 2 (GDI1 and GDI2). RAB24 was also among proteins co-precipitating with the SNARE protein Golgi SNAP receptor complex member 1 (GOSR1). Behrends et al. further validated and delineated the interaction network by identifying high-confidence candidate interaction proteins (HCIPs) using the Comparative Proteomics Analysis Software Suite (ComPASS) and its preexisting database of protein interactions, and performed comparative analysis between the HCIPs and the mass spectrometry results. RAB24 was positioned in their analysis within the NSF subnetwork, alongside multiple SNARE proteins, including GOSR1 and SNAP-29. Direct interaction was predicted between RAB24 and NSF, with NSF facilitating interactions with other proteins in the subnetwork. These results support the idea that RAB24 participates in membrane fusion. The analysis also showed RAB24 to interact

directly with GDI1 and GDI2. Interestingly, this is in contrast to observation made by Erdman et al., where they did not see any interaction between RAB24 and GDI in cultured cells (Erdman et al., 2000). HCIP analysis also showed RAB24 to interact with plakophilin-1, but the meaning of this interaction is not known.

Furthermore, many individual RAB24-interacting proteins have been reported, although the significance of these interactions is unknown. Tambe et al. reported co-precipitation of RAB24 with DRS, a tumor suppressor protein (Tambe et al., 2009). They demonstrated that DRS played a role in autophagy regulation under starvation conditions and that it was involved in the maturation of autophagosomes into autolysosomes. The interaction of RAB24 with DRS was also enhanced during autophagy induction. Schlager et al. reported weak interaction between RAB24 and Bicaudal-D-related protein 2 (BICDR-2) using GST pulldown assay (Schlager et al., 2010). Lastly, Fukuda et al. demonstrated that two RAB24 mutants—T21N and S67L—interacted with transcriptional corepressor C-terminal-binding protein 1 (CtBP1) (Fukuda et al., 2008). CtBP1 potentially functions as a transcriptional regulator and is implicated in embryonic development and in adult biological processes (Hildebrand & Soriano, 2002).

1.5 Discovering new RAB24 effectors and regulators

In order to discover new putative RAB24 effectors and regulators, Eskelinen group performed an APEX2 proximity labeling assay (Ramm et al., unpublished results). The engineered ascorbate peroxidase 2 (APEX2)-based proximity labeling assay is a method for defining the molecular environment of a protein (Nguyen et al., 2020). APEX2 is an improved, more sensitive second-generation version of the APEX enzyme. APEX proximity labeling uses the protein of interest fused with the APEX2 peroxidase. When hydrogen peroxide (H_2O_2) and biotin-tyramide (biotin-phenol) are present, APEX2 oxidizes biotin-phenols into biotin-phenoxyl radicals around the peroxidase. The radicals biotinylate nearby amino acids within several nanometers, allowing for sensitive labeling of proximal proteins around the APEX2 fusion protein. Streptavidin beads are used to enrich biotinylated proteins, which are then identified using mass spectrometry. In line with previous studies presented above, the results with Gene Ontology (GO) analysis of the APEX2 hits revealed many of the proteins near RAB24 to be associated with ER and

Golgi membranes and involved in ER-Golgi vesicular trafficking. We chose three potential interacting proteins that were among the top hits of the APEX2 assay for this thesis, to investigate their interaction with RAB24: GOLGA3, USO1 and emerin.

1.5.1 GOLGA3

GOLGA3 (formerly called golgin-160) belongs to the large protein family of golgins, that are broadly characterised by their long coiled-coil motifs and Golgi localization. Golgins appear to play a role in membrane trafficking and maintenance of Golgi structure, although their precise functions are in many cases unclear (Munro, 2011). GOLGA3 is a vertebrate-specific golgin, primarily found in the *cis*-Golgi cisternae (Hicks et al., 2006). Its functional domains include a long C-terminal coiled-coil domain, phosphorylation sites, nuclear export and import signals, and N-terminal Golgi targeting information (Hicks & Machamer, 2002). Golgin-160B is a widely expressed isoform of GOLGA3 without an exon encoding a leucine repeat sequence (Hicks & Machamer, 2005). Yadav et al. demonstrated that GOLGA3 recruits the dynein motor protein to Golgi membranes (Yadav et al., 2012). They showed that the seventh coiled-coil segment (cc7) of the C-terminal section was necessary and sufficient for dynein binding, whereas localization of GOLGA3 to Golgi membranes was mediated by GTP-bound Arf1—a small GTPase—directly binding the N-terminal end of GOLGA3. Dynein recruitment resulted in movement of the Golgi membranes towards the minus-ends of microtubules, to confer pericentrosomal Golgi positioning. GOLGA3 was absent from mitotic Golgi membranes and instead localized to the spindle poles, suggesting a mechanism for mitotic Golgi dispersal through the dissociation of GOLGA3 from mitotic membranes.

The regulation of GOLGA3 by Arf1 does not exclude further interactions with other regulatory proteins, such as RABs. Sinka et al. demonstrated that several *Drosophila melanogaster* GRIP domain golgins in the *trans*-Golgi—whose C-terminal GRIP domain binds the Arf-like 1 G protein—can also bind four different RAB proteins (Sinka et al., 2008). They also reported interaction of *Drosophila* orthologs of *cis*-Golgi golgins GM130 and GMAP-210 with RAB2 and RAB30. GMAP-210 and GM130 also bind Arf1 and GRASP65, respectively, via their C termini. In addition, Golgi dispersal and

positioning are relevant in cancer research, as disruption and fragmentation of Golgi dynamics is one of the hallmarks of many cancer cells (Bui et al., 2021).

1.5.2 USO1

USO1 (also called p115) is a peripheral membrane protein of the golgin family, with a coiled-coil domain, two globular head domains and an acidic tail region, structurally reminiscent of myosin II (Sapperstein et al., 1995). It localizes to ER exit sites, the vesicular-tubular clusters (VTCs) and the *cis*-Golgi (Nelson et al., 1998; Waters et al., 1992). USO1 is one of the most studied golgins and has been shown to participate in several membrane trafficking steps as a molecular tether. It was first shown to be necessary for transcytosis and the tethering of intra-Golgi membrane vesicles (Barroso et al., 1995). Later studies revealed that USO1 was also required for ER–Golgi traffic, as depletion of USO1 led to the accumulation of vesicular stomatitis virus (VSV) glycoprotein (VSV-G) in peripheral VTCs (Alvarez et al., 1999). USO1 is a direct effector of RAB1, which recruits USO1 to coat protein complex II (COPII) vesicles as they bud from the ER (Allan et al., 2000). Recruitment of USO1 to COPII vesicles might also depend on the assembly status of the vesicle SNAREs (Brandon et al., 2006). Further support for the role of USO1 as a tethering factor comes from experiments with the yeast homolog of USO1—Uso1p— as it was found to be an essential component of yeast ER–Golgi trafficking by tethering COPII vesicles to Golgi membranes (Barlowe, 1997; Nakajima et al., 1991). It was suggested that the Uso1p tethering process is independent of SNAREs, as it remained unaffected when SNARE function was inhibited using inactive SNARE mutants or inhibitory anti-SNARE antibodies. (Cao et al., 1998). Despite their inhibited ability to catalyze vesicle fusion, SNAREs remained present and might still be involved in the tethering process. Indeed, a later study found that monomeric ER/Golgi SNAREs Sec22b and Rbet1 interacted stably with USO1, potentially functioning as USO1 binding sites on COPII vesicles (Wang et al., 2015). In addition to tethering COPII vesicles, USO1 has been shown to be important for tethering COPI vesicles to Golgi membranes (Sönnichsen et al., 1998). USO1 also participates in the reassembly of Golgi cisternae after mitosis (Nakamura et al., 1997).

Despite the extensive research of USO1, its exact roles in the tethering processes are still unknown. However, it is known that USO1 operates by interacting with many other proteins in addition to SNAREs and RAB1, namely the golgins GOLGA2 (also called GM130) and giantin, and the multisubunit complexes COG (conserved oligomeric Golgi) and TRAPP (transport protein particle) (Wang et al., 2015). Additionally, Yoon et al. discovered an alternatively spliced *USO1* RNA-transcript, whose expression was linked to poorer prognostic outcomes in HCC patients. This transcript also promoted a more malignant form of HCC *in vivo* and *in vitro* (Yoon et al., 2021).

1.5.3 Emerin

Emerin is unique among the candidate RAB24 interactors, because it is a protein that associates with the nuclear envelope. It was first identified as the gene responsible for the X-linked form of Emery-Dreifuss muscular dystrophy (EDMD) (Bione et al., 1994). Emerin localizes predominantly to the inner nuclear membrane (INM), although it has also been detected in the outer nuclear membrane (ONM) and in VTCs (Berk et al., 2013). Emerin is a part of the LAP2-emerin-MAN1-domain (LEM) protein family. LEM-domain containing proteins are fundamental components of the nuclear lamina; a thin meshwork of lamin intermediate filaments located inside the INM. The nuclear lamina supports the nucleus mechanically. It also contributes to genome stability, DNA replication and gene regulation by providing a scaffold for various protein interactions (Gerace & Huber, 2012).

Emerin binds to at least 16 other proteins, and the various binding partners suggest that emerin may function as an integrating factor for a variety of mechanical and signaling inputs, subsequently converting these inputs into circumstances that can lead to appropriate changes in gene activity (Berk et al., 2013). Among the interacting partners of emerin are lamin A, lamin C and Barrier-to Autointegration Factor (BAF) which, together with LEM-domain proteins, are necessary for the postmitotic assembly of the nuclear lamina (Margalit et al., 2005). Vaughan et al. found that in the absence of lamin A, emerin and lamin C mis-localized to the ER, suggesting that lamin A is required for anchoring lamin C and emerin to the INM and nuclear lamina (Vaughan et al., 2001). The double stranded DNA (dsDNA) binding protein BAF is directly bound by the LEM-

domain of emerin (Lee et al., 2001). BAF is a highly conserved protein in multicellular eukaryotes, involved in various cellular functions such as gene transcription regulation and chromatin organization, roles in which emerin may also participate (Margalit et al., 2007). Emerin also binds directly the two transcription factors Lim-domain-only 7 (Lmo7) and β-catenin, further supporting a role for emerin as a transcription regulator (Markiewicz et al., 2006; Melcon et al., 2006). β-catenin is a well-known protein that mediates the canonical Wnt signaling pathway. In emerin-null fibroblasts, β-catenin accumulates at high levels in the nucleus, accompanied by increased β-catenin activity. Consequently, the cells grow rapidly and proliferate even in low serum conditions, suggesting that under normal conditions emerin attenuates Wnt signaling (Markiewicz et al., 2006). Similarly, emerin appears to inhibit the nuclear accumulation of Lmo7. Lmo7 activates the emerin gene, with evidence suggesting mutual feedback regulation between Lmo7 and the emerin protein (Melcon et al., 2006). Emerin also binds directly to histone deacetylase 3 (HDAC3), the catalytic subunit of the nuclear co-repressor (NCoR) complex, recruiting HDAC3 to the nuclear periphery and stimulating its activity (Demmerle et al., 2012). HDACs remove acetyl groups from histones, decreasing chromatin accessibility for transcription factors and repressing gene expression (Milazzo et al., 2020). Emerging evidence suggests that emerin plays a role in tissue-specific gene silencing through its interaction with HDAC3 (Berk et al., 2013; Demmerle et al., 2012).

Emerin is also implicated in nuclear movement and polarity. Actin-dependent nuclear movement is mediated by the linker of nucleus and cytoskeleton (LINC) complex which traverses the nuclear envelope. (Gundersen & Worman, 2013). The LINC complex connects to the cytoskeleton via nesprin proteins in the ONM, and to the nuclear lamina via SUN proteins in the INM (Folker et al., 2011). In migratory fibroblasts the nucleus polarizes via SUN2 and nesprin-2G, that arrange into transmembrane actin-associated nuclear (TAN) lines (Luxton et al., 2010). The INM protein SAMP-1 is also suggested to be a component of TAN-lines, as it localizes to TAN-lines and is required for nuclear movement in fibroblasts (Borrego-Pinto et al., 2012). TAN-lines attach to the nucleus via lamin A/C and SUN2, allowing the forces exerted by the actin filaments of the cytoskeleton to be transferred to the nucleus (Folker et al., 2011). Emerin interacts with SAMP-1 and the LINC complex components SUN1 and SUN2, as well as with nesprin-1 and nesprin-2 (Haque et al., 2010; Zhang et al., 2005). Emerin also directly binds to and caps the pointed ends of actin filaments, stabilizing them *in vitro* (Holaska et al., 2004).

Chang et al. demonstrated that emerin interacts with myosin IIB, and together they are required for the polarization of actin flow and nuclear movement in fibroblasts (Chang et al., 2013). Later studies showed that emerin knockdown abolished the polarized distribution of several nuclear envelope proteins, indicating that emerin is crucial for nuclear polarity (Nastały et al., 2020). Emerin has also been shown to interact with tubulin and the centrosome. Emerin knockdown resulted in the disassociation of the centrosome from the nuclear envelope, suggesting a role for emerin in organizing the microtubule cytoskeleton (Salpingidou et al., 2007). Finally, Wu et al. demonstrated that emerin knockdown facilitated HCC cell migration and invasiveness *in vitro* and metastasis *in vivo* (Wu et al., 2022).

1.6 Objectives of the work

In summary, RAB24 is a unique member of the RAB protein family, with important differences compared to other RAB proteins. It plays a role at the later stages of the autophagic and endocytic degradation pathways, and is essential for Purkinje neuron survival. Normal cell division also requires RAB24. In hepatocytes, RAB24 affects cellular energy metabolism, potentially through influencing mitochondrial dynamics, and is associated with diseases such as HCC. Still, the exact functional mechanisms of RAB24 are unknown, and crucial in this regard is to identify its effector proteins that mediate these functions. Several putative interacting and/or effector proteins have been found to associate with RAB24, but further research is still needed to clarify the molecular mechanisms of RAB24.

This thesis investigates the association of RAB24 with three new putative interacting proteins; GOLGA3, USO1 and emerin. Our methodical approach is twofold: Firstly, physical interaction between the interactor and RAB24 is investigated using co-immunoprecipitation. Secondly, immunofluorescence imaging with confocal microscopy is used to investigate the localization—and the potential co-localization—of the proteins within the cell, and co-localization is quantified with image analysis software.

2 Materials and methods

2.1 Cell culturing and transfections

RAB24-knockout Huh-7 cell line was primarily used in the experiments of this thesis. Preliminary antibody testing was performed using wild-type Huh-7 and Hep G2 cell lines. The Huh-7 cell line was created in 1982 from a hepatocyte-derived carcinoma, operated from the liver of a 57-year-old Japanese male (https://huh7.com/). The Hep G2 cell line also originates from liver cells, operated from the liver of a 15-year-old Caucasian male with hepatocellular carcinoma (https://www.cytion.com/). Similar to RAB24, USO1 and emerin have a demonstrated association with HCC malignancy (Z. Chen et al., 2017; Wu et al., 2022; Yoon et al., 2021), and GOLGA3 affects Golgi dynamics, which are known to be altered in many types of cancers (Bui et al., 2021; Yadav et al., 2012). Huh7 and Hep G2 cell lines were selected for their relevance in this context.

RAB24-knockout Huh-7 cell line was produced by Lav Tripathi using the CRISPR/Cas9 technology, prior to the experiments of this thesis. The cells were cultivated in standard +37 °C and 5 % CO_2 environment in T75 flasks. The cell medium used was α-MEM with added supplements (Appendix 1). The cells were regularly split in a 1:5 ratio when nearing confluency. Huh-7 is an adherent cell line, and during sub-culturing the cells were incubated in trypsin solution (0,25 % trypsin, 0,02 % potassium-EDTA) for 5 minutes, to detach them from the bottom of the flask. After that, the cells were resuspended in 10 ml of fresh media.

In order to compare RAB24-expressing cells and knockout cells in the experiments, transient transfections were performed for the RAB24-knockout Huh-7 cells with two different plasmids, to create a treatment and a control group. The treatment group was transfected with a plasmid containing a GFP-RAB24 construct, whereas the control group was transfected with a GFP-Empty plasmid, and thus did not express RAB24 (Appendix 2). The GFP-RAB24 and GFP-Empty plasmids were constructed by Lav Tripathi prior to the experiments of this thesis. For the purposes of this thesis, however, the plasmids were propagated in *E. coli* cultures and extracted and purified using a Nucleobond® Midiprep

kit according to the manufacturers protocol (Appendix 3). The plasmids were stored at -20 °C. The transfections were performed the day before each experiment using the jetOPTIMUS® transfection reagent, according to the manufacturers protocol (Appendix 4).

2.2 Co-immunoprecipitation

Co-immunoprecipitation (co-IP) was used to study the physical interaction between RAB24 and the three potential effector proteins. Co-immunoprecipitation is a widely used method for studying protein-protein interactions (Takahashi, 2015). It uses microscopic beads coupled to antibodies for a specific target protein, to capture and precipitate the target proteins from a sample. Any proteins physically interacting, directly or indirectly, with the primary target proteins are precipitated with the primary target. After removing any unbound proteins with a series of washes, the resulting complexes are analyzed by immunoblotting.

For co-IP 2 million cells were seeded in two 100-mm cell culture dishes and grown for 24 h. The following day, the transient transfections were performed using the jetOPTIMUS® transfection reagent (Appendix 4). Per culture dish, 10 µg DNA and a 1:1 ratio of DNA and jetOPTIMUS® reagent was used, and the mixture was added on the cells for 24 h. Transfection efficiency was visually assessed with a fluorescence microscope using the GFP signal intensity as a marker for successful transfection. After this, the cells were processed for co-IP. First, the medium was aspirated from the dishes and the cells were washed with 10 ml of PBS per dish. Then the cells were incubated in 1 ml of trypsin (0,25 % trypsin, 0,02 % potassium-EDTA) for 5 minutes to detach the cells. After the incubation, 10 ml of fresh medium was added per dish. The cells were detached from the bottom and released into the medium by pipetting up and down several times around the dish. The detached cells were collected in separate 15 ml falcon tubes and centrifuged at 420 RCF/4 minutes at +4 °C. After this, the medium was removed and the remaining cell pellet was resuspended to 10 ml of PBS, following another centrifugation at 420 RCF/4 minutes at +4 °C. After the centrifugation, the PBS was removed and 500 µl of co-IP lysis buffer (Appendix 1) was added per falcon tube. The cells were lysed by pipetting the suspension up and down several times, and then the

suspension was left at +4 °C for 15 minutes. After the incubation, the lysates were centrifuged at 420 RCF/10 minutes at +4 °C, and the supernatants were collected in two Eppendorf tubes and kept on ice.

Next, protein concentration was estimated for the supernatants using the BCA kit, as per the manufacturers protocol (Pierce™ BCA Protein Assay Kit, Thermo Scientific, 23225). Absorbance measurement was done at 562 nm using the Ensight™ Multimode Microplate Reader (PerkinElmer). For co-IP, anti-GFP magnetic beads (ChromoTek GFP-Trap® Magnetic Agarose) were used to precipitate the GFP-RAB24 and GFP-Empty constructs. First, 30 µl of anti-GFP beads were pipetted into empty Eppendorf tubes. Next, the beads were separated from their stock buffer using a magnetic Eppendorf stand, to hold the beads in place as the buffer was aspirated using a pipette. After this, the beads were diluted in 500 µl of wash buffer (Appendix 1), to equilibrate the beads with the buffer. The wash buffer was then discarded in the same fashion as the stock buffer, using the magnetic stand. Next, the volume of lysates was adjusted so that they had the same protein concentration. After that, the lysates were added to the beads. Due to inconsistencies in the protein yield extracted from the lysed cells, there was variability in the total protein content of the lysates, ranging from 600 µg to 2,5 mg. The amount of protein loaded onto the beads is an important variable in co-IP because the amount of interacting proteins may be too low for detection if there is not enough total protein in the lysate. Importantly, before adding the lysate onto the beads, 10 µg of protein from both lysates was extracted and stored for later analysis.

Next, the lysate was allowed to incubate with the beads for 1 h at +4 °C in a tube rotator. Post incubation, the lysates were centrifugated at 500 g/5 minutes at room temperature (RT) to bring down excess liquid droplets stuck on the Eppendorf lid. After that, the beads were separated from the supernatant using the magnetic Eppendorf stand. The remaining supernatant (flow-through) was stored for later analysis. Next, the beads were washed three times with 500 µl of wash buffer. The last washing step was carried out in a separate fresh Eppendorf tube. Then, to prepare the samples for SDS-PAGE, 25 µl of 2X-Laemmli buffer (Appendix 1) was added to the beads. Similarly, the two other samples were also prepared at this time; the initial lysate sample that was collected before adding the beads, and the flow-through sample. After adding the Laemmli buffer, all samples were boiled at +95 °C for 10 minutes using a dry block heater. After that, the samples were centrifuged

to bring down the condensed liquid droplets stuck on the Eppendorf lid. All the samples were stored at +4 °C.

Next, a 1.5 mm thick 10 % SDS-PAGE gel was prepared, and the samples were loaded into the wells. The total volume of the co-IP samples was loaded, whereas for the initial lysate and flow-through samples, 10 µg was loaded. Molecular weight protein ladder (1,5 µl) was also loaded (PageRuler® Plus Prestained Protein Ladder, Thermo Fisher, 26619). The gel initially ran at 90 V for 30 minutes, after which the voltage was increased to 140 V for 60 minutes or until the tracking blue dye reached the bottom of the gel. After the run, the gel was incubated in transfer buffer for 15 minutes on a shaker. The transfer buffer and running buffer recipes are found in Appendix 1. For the subsequent western blot, a PVDF membrane was activated in methanol for 2 minutes and incubated in transfer buffer for 10 minutes on a shaker. A wet transfer was then performed at 90 V for 90 minutes at +4 °C.

After the transfer, the PVDF membrane was carefully inserted into a 50-ml Falcon tube and blocked overnight at +4 °C in a tube rotator, using a 5 % non-fat dry milk powder (NFDM), diluted in TBST (Appendix 1). After blocking the membrane, immunostaining was performed using antibodies listed in Table 1. The antibodies were diluted in 5 % NFDM/TBST solution. The membrane was incubated with a primary antibody for 1.5 h at RT in a tube rotator, after which the membrane was washed three times in TBST, each wash incubating for 5 minutes. Then, the membrane was incubated with a HRP-conjugated secondary antibody for 1 h at RT in a tube rotator, followed by another 3 x 5 minutes TBST wash. After that, the membrane was placed on a rack and a chemiluminescent substrate (Clarity Max Western ECL Substrate, Bio-Rad, 1705062) was added to the membrane, followed by a 3-minute incubation. Subsequently, the chemiluminescence was imaged using Sapphire Biomolecular Imager (Azure Biosystems) with cumulative exposure time. After imaging, the membrane was stripped from antibodies, to allow further immunostaining. The membrane was first stained and imaged with GOLGA3, USO1 or emerin antibodies, then stripped, and after that stained and imaged with GFP antibodies, to confirm that the co-IP protocol was successful. Membrane stripping was performed by first rinsing the membrane with Milli-Q water, and then incubating it in stripping solution (Appendix 1) for 20 minutes in a shaker. After the first incubation, a 10-minute incubation in fresh stripping solution followed, after

which the membrane was stored overnight in 5 % NFDM/TBST solution at +4 °C in a tube rotator. GFP staining and imaging were performed the next day following the same protocol as described above.

Table 1. The following antibodies were used in western blot immunostaining.

Primary antibody	Host	Manufacturer, catalog number	Dilution
Emerin monoclonal α-human	Mouse	Invitrogen, MA5-31327	1:1000
GOLGA3 polyclonal α-human	Rabbit	Proteintech, 21193-1-AP	1:1000
USO1 monoclonal α-human	Rabbit	Invitrogen, MA5-44748	1:1000
Anti-GFP	Mouse	Roche, 11814460001	1:1000
Secondary antibody	Host	Manufacturer, catalog number	Dilution
HRP-conjugated α-Rabbit-IgG	Goat	Jackson ImmunoResearch, 111-035-003	1:10 000
HRP-conjugated α-Mouse-IgG	Goat	Jackson ImmunoResearch, 115-035-003	1:10 000

2.3 Immunofluorescence staining

Immunofluorescence staining was performed in order to study potential co-localization of RAB24 with the three protein candidates. The samples were imaged using confocal microscopy, and statistical analyses measuring co-localization were conducted using the image data. Co-localization of proteins to the same compartments and structures within the cell, and especially a positive correlation in their abundance wherever they co-localize, provides further support for a functional relationship between the proteins (Aaron et al., 2018). This is why a co-localization analysis complements the results of co-immunoprecipitation, and provides more confidence in determining protein interaction.

Immunofluorescence staining started by placing 13-mm coverslips at the bottom of wells in a 12-well culture plate. Then, 200 000 cells were seeded per well and left to grow overnight in an incubator at +37 °C and 5 % CO_2. Half of the wells were transfected with a GFP-RAB24 plasmid, and the other half with a GFP-Empty plasmid. The transfection was performed with the jetOPTIMUS® reagent as per the manufacturers protocol (Appendix 4). 1 µg of DNA and a 1:1 ratio of DNA and jetOPTIMUS® reagent was used,

and the mixture was left on the cells for 24 h. Transfection efficiency was assessed visually using the GFP fluorescent signal.

After the transfection, the cells were processed for immunostaining. Medium was aspirated from the wells and the cells were washed once with PBS. Next, the cells were fixed using 1 ml of 4 % paraformaldehyde (PFA) solution in PBS per well. The cells were incubated in PFA for 20 minutes at RT. After the fixation, the cells were washed once with PBS, followed by permeabilization with 1 ml of 0,2 % Triton X-100 in PBS for 30 minutes at RT. After the permeabilization, the cells were washed twice with PBS. Next, the cells were blocked using 1 % BSA in PBS for 30 minutes at RT, to inhibit unspecific binding of antibodies. After the blocking, immunostaining was performed by adding 50 µl drops of primary antibody solution on parafilm, and the coverslip placed on top of the solution, with the side with cells facing down, using tweezers. Antibodies and their dilutions are listed in Table 2. The antibodies were diluted in 1 % BSA/PBS. Before placing the coverslip on top of the antibody solution, excess liquid was removed by touching the side of the coverslip on tissue paper. After placing the coverslips on the parafilm, they were left to incubate for 1 h at RT, covered from light. After the incubation, the coverslips were washed by adding three 1 ml drops of PBS on the parafilm, and placing the coverslip on the drop, one after the other. Between the washes, the coverslip was dried by touching its side on tissue paper. After washing the coverslips, they were then incubated with fluorescent secondary antibodies (Table 2.), using the same protocol as with the primary antibodies. Then, the coverslips were washed in PBS. After washing, 50 µl of Mowiol mounting solution with DAPI (Appendix 1.) was added on microscope slides and the coverslips were placed on top of the slides. The slides were left to dry overnight at RT covered from light, after which they were transferred to +4 °C.

Table 2. The following antibodies were used in immunofluorescence staining.

Primary antibody	Host	Manufacturer, catalog number	Dilution
Emerin monoclonal α-human	Mouse	Invitrogen, MA5-31327	1:100
GOLGA3 polyclonal α-human	Rabbit	Proteintech, 21193-1-AP	1:25
USO1 monoclonal α-human	Rabbit	Invitrogen, MA5-44748	1:50
Secondary antibody	Host	Manufacturer, catalog number	Dilution
Alexa Fluor Plus 647-conjugated α-rabbit-IgG	Goat	Invitrogen, A32733	1:500
Alexa Fluor Plus 647-conjugated α-Mouse-IgG	Goat	Invitrogen, A32728	1:500

2.4 Imaging and co-localization analysis

The slides were imaged with a 3i spinning disk confocal microscope (Marianas CSU-W1), with Photometrics Prime BSI sCMOS camera, Zeiss alpha Plan-Apochromat 100x/1.46 NA oil DIC M27 objective, and the SlideBook 6 application. GOLGA3, USO1 and emerin—stained with the Alexa Fluor 647 secondary antibodies—were imaged using a 640-nm excitation wavelength, whereas GFP and DAPI were imaged with 488-nm and 405-nm excitation wavelengths, respectively. The cells were imaged in optical sections with image z-stack step size of 0,23 µm and exposure time 100 ms. A total of 30 cells from GOLGA3 and USO1 stained cells were imaged, 15 from GFP-RAB24 cells and 15 from GFP-Empty cells. Emerin-stained cells were excluded from further co-localization analysis, due to highly unexpected staining pattern with the antibody.

Due to a significant chromatic shift in the microscope, we post-aligned our image data using the Chromagnon software, with a transformation matrix generated by imaging 200-nm Tetraspeck Microspheres (for further information, see Matsuda et al., 2018). Pearson's coefficient and Mander's coefficient were used to quantify co-localization. This In order to remove diffuse background signal from the images before the co-localization analysis, image data was processed by subtracting the average signal intensities from the 488 and 640 channels, so that only the signal above the average threshold remained. Due to lower signal intensity in the USO1/640 channel, a value of 0.8 times the average intensity was subtracted for USO1-labelled samples for Pearson's coefficient. Conversely, in the USO1 Manders' correlation measurement, 1.1 times the average was subtracted, due to the saturation of the M2 metric (multiple values at the maximum correlation value of 1).

After pre-processing the images, co-localization of the 488-nm GFP signal with the 640-nm signal from USO1 and GOLGA3 was analyzed using the Coloc2 plugin in ImageJ. The plugin measures the two correlation coefficients: the Pearson's coefficient r and the two Manders' coefficients, M1 and M2. Pearson's and Manders' coefficients measure co-localization in different manners (Aaron et al., 2018). Pearson's coefficient calculates the correlation in signal intensity at every pixel where the signals overlap, thus providing information about the correlation of protein abundance in a specific location. It provides values between -1 and 1, where -1 signifies a perfect negative correlation and 1 perfect

positive correlation. Manders' coefficients M1 and M2, on the other hand, measure the spatial co-occurrence, or overlap, of the two signals, without being affected by the intensities of the signals, with values ranging from 0 of no overlap, to 1 of total overlap. In this experiment, the M1 coefficient measured the proportion of pixels positive for the GFP/RAB24 signal that were also positive for the USO1/GOLGA3 signal and, conversely, the M2 calculated the proportion of USO1/GOLGA3-positive pixels that were also positive for GFP/RAB24 signal.

As all the correlation measurement data sets were normally distributed—determined with the Jarque-Bera test—we used the Student's *t*-test with one-tailed distribution and equal variance, to compare the means of the measurements between the treatment and the control groups. The p-value of 0.05 was assigned as the limit for statistical significance. Statistical tests were performed using Microsoft Excel, and graphs were created in the Origin software (2016 edition).

3 Results

3.1 No consistent co-immunoprecipitation of USO1, GOLGA3 and emerin with RAB24

In order to study the physical interaction between RAB24 and the three putative interacting protein candidates USO1, GOLGA3 and emerin, I used the co-immunoprecipitation technique. With sample total protein content of 600 or 700 µg, no co-precipitation was observed between any of the candidate proteins and RAB24 (results not shown). Similarly, with 1-mg sample protein content, emerin and USO1 displayed no co-immunoprecipitation (Figure 2A). GOLGA3 was not tested with this total protein content. An experiment with 2 mg total protein content, on the other hand, showed co-immunoprecipitation with all of the candidate interactors (Figure 2B). In another experiment with total protein content of 2.5 mg, emerin and GOLGA3 showed a signal in the precipitated samples (Figure 2C). However, the same signal was seen in both the GFP-Empty and GFP-RAB24 samples, suggesting non-specific binding to the beads. USO1 was not tested in this experiment. GOLGA3 consistently displayed two different bands in the blots—possibly two protein fragments—one with the expected molecular weight of 167 kDa, and another of roughly 100 kDa (Figure 2B and C). Emerin also displayed an additional band slightly larger than the expected 29 kDa in the input sample of the 1-mg and the 2.5-mg experiments (Figure 2A and C), as well as in the precipitate sample of the 2-mg and the 2.5-mg experiments (Figure 2B and C). In addition, some of the GFP-RAB24 fusion protein was degraded, made apparent by bands in the GFP-RAB24 samples at a size of roughly 27 kDa (Figure 2A, B and C), which is the size of the individual GFP protein.

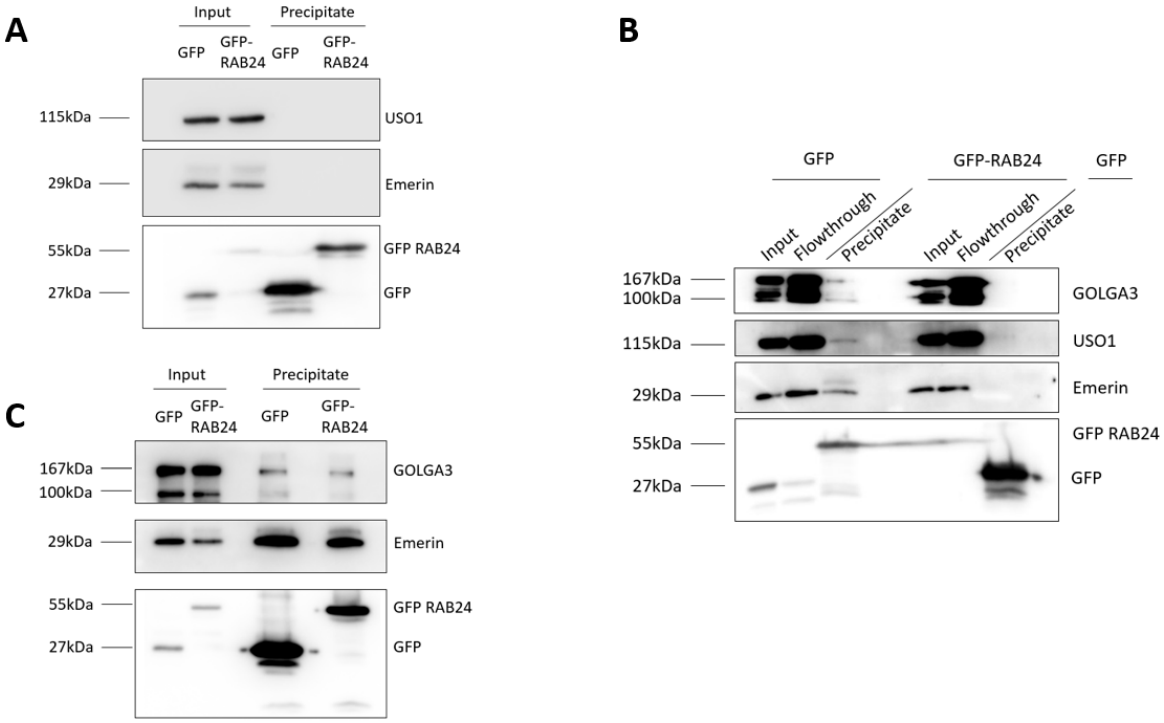

Figure 2. Testing co-immunoprecipitation of GOLGA3, USO1 and emerin with RAB24, using sample protein contents of 1 mg (A), 2 mg (B) and 2.5 mg (C). RAB24-knockout Huh7 cells were transfected with either a GFP-RAB24 plasmid or a GFP-Empty plasmid. **A.** This experiment did not show co-immunoprecipitation of USO1 and emerin with GFP-RAB24. **B.** Note that the precipitate samples were loaded in an inverse order; the GFP-RAB24 precipitate is adjacent to the GFP-Empty input and flow-through samples, and vice versa. This experiment showed co-immunoprecipitation of GOLGA3, USO1 and emerin with GFP-RAB24 but not with GFP. **C.** This experiment showed co-immunoprecipitation of GOLGA3 and emerin with both GFP-Empty and GFP-RAB24, suggesting non-specific binding to the GFP-Trap beads.

3.2 USO1 co-localized more with RAB24

In order to investigate whether RAB24 co-localized within the cell with GOLGA3, USO1 and emerin, I used immunofluorescence microscopy to compare the cellular co-localization of the proteins with GFP-RAB24, and GFP as a control. Emerin was excluded from this analysis due to the unexpected staining pattern observed with the antibody. The anti-emerin displayed a signal with ubiquitous cytoplasmic localization, as opposed to the expected localization mainly in the nuclear envelope (Figure 3.).

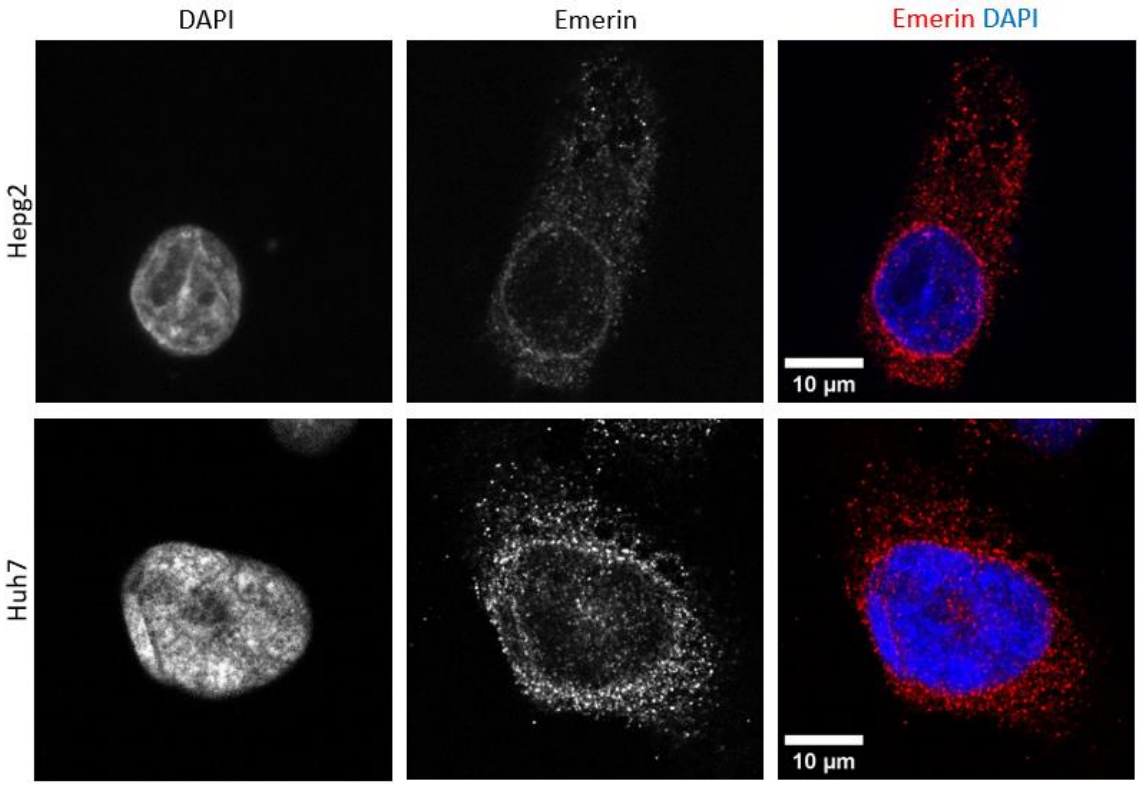

Figure 3. Anti-emerin displayed a ubiquitous cytoplasmic localization, as opposed to the expected localization mainly in the nuclear envelope. For this reason, emerin was excluded from co-localization analysis. Single-plane confocal microscope images of immunofluorescence-stained Huh7 and Hepg2 cells, with emerin in red and the nucleus in blue (DAPI).

For GOLGA3, no significant difference was observed in its co-localization with GFP and GFP-RAB24, as measured with the Pearson's coefficient and the Manders' coefficient M1 (Figure 4A, B and C). On the other hand, Manders' coefficient M2 (Figure 4D) was significantly different between GFP-RAB24 and GFP, however, GFP displayed more co-localization with GOLGA3 than GFP-RAB24.

USO1 was found to co-localize more with GFP-RAB24 compared to GFP, as measured with the Pearson's coefficient and the Manders' coefficient M1 (Figure 5A, B and C). Manders' coefficient M2 showed no significant difference between the two samples (Figure 5D).

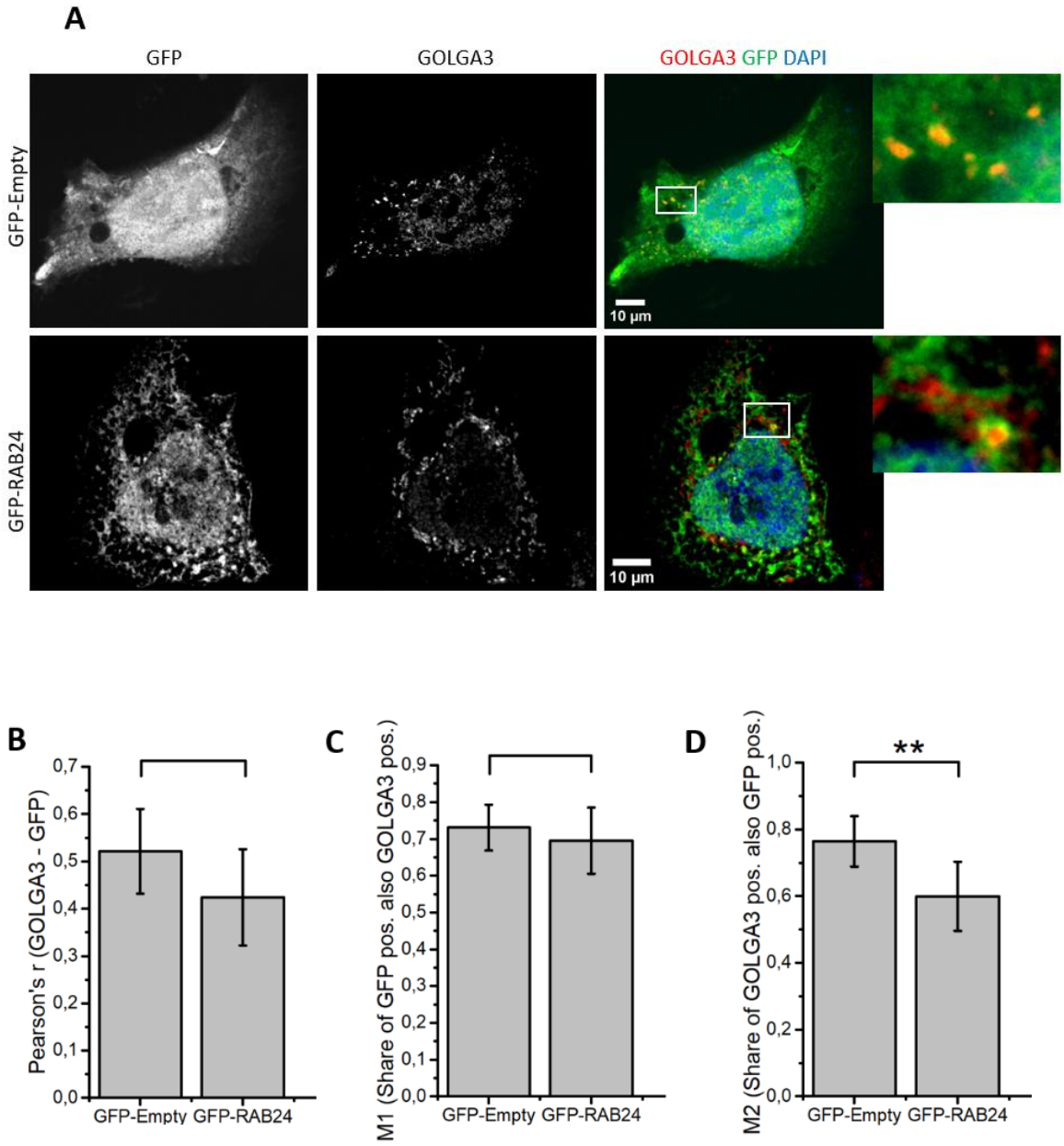

Figure 4. Co-localization of endogenous GOLGA3 with GFP-RAB24 and GFP. RAB24-knockout Huh7 cells were transfected with either GFP-RAB24 or GFP-Empty plasmids. **A.** Single-plane confocal microscope images of immunofluorescence-stained Huh7 cells, with GOLGA3 in red, GFP in green and the nucleus in blue (DAPI). Co-localization of GOLGA3 and GFP/GFP-RAB24 appears as orange to yellow. No significant difference in co-localization was found between GOLGA3 and GFP-RAB24 compared with GOLGA3 and GFP, as measured with (**B**) Pearson's correlation coefficient r or (**C**) Manders' coefficient M1. **D.** Manders' correlation coefficient M2 was significantly higher ($p < 0,01$) for GOLGA3 and GFP, suggesting that the GFP co-localized more with GOLGA3 compared with GFP-RAB24. The error bars display the margin of error within a 95 % confidence interval.

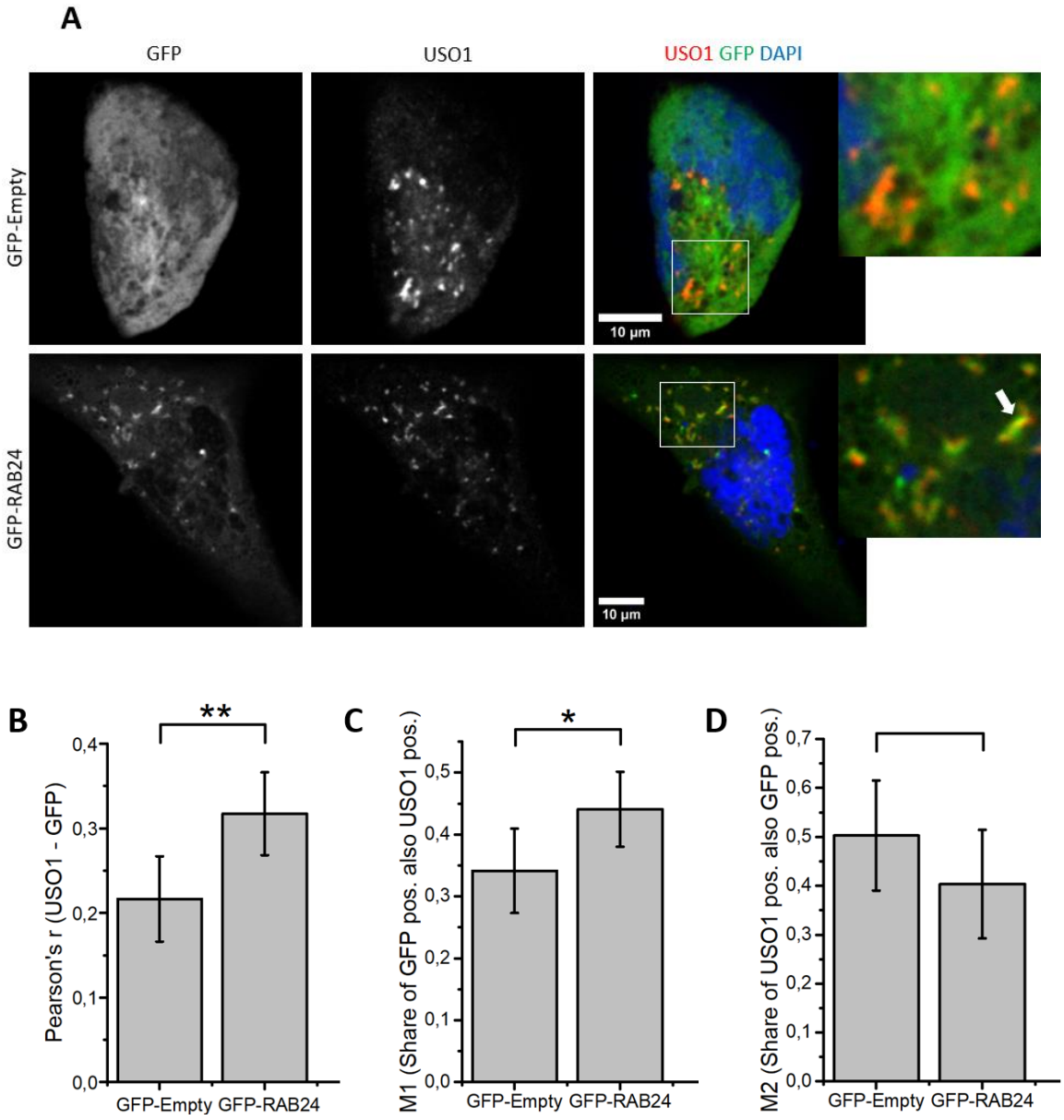

Figure 5. Co-localization of endogenous USO1 with GFP-RAB24 and GFP. RAB24-knockout Huh7 cells were transfected with either GFP-RAB24 or GFP-Empty plasmids. **A.** Representative single-plane confocal microscope images of immunofluorescence-stained Huh7 cells, with USO1 in red, GFP in green and the nucleus in blue (DAPI). Co-localization of USO1 and GFP/GFP-RAB24 appears as yellow-to-orange. The arrow indicates a clear co-localization of USO1 with GFP-RAB24. **B.** GFP-RAB24 co-localized with USO1, as the Pearson's correlation coefficient r was significantly higher ($p < 0,01$) in the GFP-RAB24. **C.** The Manders' correlation coefficient M1 was also significantly higher for GFP-RAB24 ($p < 0,05$), while (**D**) the Manders' coefficient M2 was not statistically different between GFP-RAB24 and GFP. The error bars display the margin of error within a 95 % confidence interval.

4 Discussion

4.1 Optimizing co-immunoprecipitation

In this thesis, I investigated the relationship between RAB24 and its three potential interactors GOLGA3, USO1 and emerin, using co-immunoprecipitation, and immunofluorescence imaging with confocal microscopy. My results with co-immunoprecipitation were inconclusive. In one experiment, all three proteins co-precipitated with GFP-RAB24 while no precipitation was observed with GFP as expected. However, the positive results could not be repeated in two other experiments. It is important to note, however, that in the negative co-IP experiments, the amount of total protein in the sample lysates was lower, which could have an effect on the results. In one experiment, GOLGA3 and emerin precipitated with both the GFP-RAB24 and the GFP control, suggesting that this result was due to non-specific binding to the beads, instead of interaction with RAB24.

There are several possible reasons for the contradictory co-IP results. One possibility is that the co-IP protocol is not sufficiently optimized for the proteins under investigation, as protein-protein interactions can be very dynamic and/or labile and can easily be disturbed by unsuitable conditions during the protocol, leading to false negative results (Morató et al., 2021). In this regard, selection of an appropriate lysis buffer is a critical factor. The lysis buffer contains a detergent that is used in the first step of cell lysis. It ideally only disturbs the cellular membranes and lipid-protein interactions of the cells, and thus allows proteins of interest to be released into the lysate, without affecting the protein-protein interactions that are under investigation. Generally, ionic detergents tend to affect both protein-protein and lipid-protein interactions, whereas non-ionic detergents, such as NP-40 and Triton X-100 disrupt only lipid-protein interactions (Takahashi, 2015). In line with this, I used NP-40 as a detergent in the lysis buffer (Appendix 1). However, to further optimize the protocol, the detergent content in the wash buffer used in the subsequent steps after cell lysis could be diluted (Appendix 1), as this could better preserve easily disturbed interactions between the proteins under investigation. Indeed, Lav Tripathi performed a positive co-IP with reduced NP-40 content in both the lysis

buffer (0.5 %) and the wash buffer (0.25 %), where emerin precipitated with GFP-RAB24 but not with GFP. For GOLGA3 and USO1, no precipitation was observed with either GFP-RAB24 or GFP.

Also, if the protein-protein interactions are weak or occur at low endogenous levels, it is possible to increase the detection sensitivity by overexpressing the proteins of interest. RAB24 can already be considered overexpressed in these experiments, as the GFP-RAB24-expressing cells were produced by transiently transfecting with the pEGFP-C1 plasmid (Appendix 2). In addition to GFP-RAB24, the potential interacting protein could also be overexpressed, to allow possible weak interactions to be detected. It is important to note, however, that overexpression can also lead to non-physiological interactions and false positive results, so these types of results should be interpreted accordingly, and ideally confirmed in a more physiologically relevant context (Evans & Paliashvili, 2022).

Protein crosslinking could also be used to identify transient or weak protein-protein interactions. In crosslinking, two or more proteins are covalently joined together via a crosslinker. Crosslinkers are reagents containing reactive groups that form covalent bonds with specific amino acid residues on proteins. This process ‘freezes’ protein-protein interactions in place, allowing for the isolation and characterization of weak and/or transient protein complexes (Wang et al., 2019).

The relatively large GFP-tag in the GFP-RAB24-expressing cells might also affect the results. The GFP-RAB24 construct is roughly double the size of the wild-type RAB24 protein, and this could potentially interfere with the molecular interactions of RAB24 (Schneider & Hackenberger, 2017). The GFP-tag is useful because it enables the use of highly specific nanobodies against the GFP protein (GFP-Trap) to precipitate the GFP-RAB24 construct from the sample, with limited cross-reactivity with any unwanted proteins. However, the GFP-tag could be substituted for a smaller one—such as FLAG or Myc-tag—that would still enable the use of specific tag antibodies. Using antibodies against RAB24 for co-IP has proven to be problematic, as it has resulted in high levels of unspecific binding (our unpublished results).

Another possible reason for the negative results could be the fact that the APEX2 proximity assay used for identifying proteins in close proximity to RAB24, was

performed using the mouse Neuro2a cell line, while the human Huh-7 cell line was used in the experiments of this thesis. It is possible that the three candidates GOLGA3, USO1 and emerin localize nearby, and potentially interact with RAB24 in Neuro2a cells, but not in Huh-7 cells. However, considering the highly conserved nature of RAB proteins across species, especially within mammals, this is not likely (Krishnan et al., 2020).

4.2 Interpreting co-localization

The results from the co-localization analysis were also mixed. Firstly, emerin was excluded from the co-localization analysis, due to an unexpected staining pattern of the antibody in immunofluorescence staining. Second, for GOLGA3, no difference in co-localization was observed between the GFP-RAB24 and GFP, except the Manders' M2 coefficient. In this case, however, the co-localization was higher for GFP than for GFP-RAB24, which shows that there is no co-localization of GOLGA3 with GFP-RAB24. USO1, on the other hand, co-localized with GFP-RAB24 more than GFP, when monitored with Pearson's correlation coefficient and with Manders' coefficient M1. Importantly, when assessing whether two molecules could interact with each other, Pearson's coefficient is a better metric. This is because the guiding assumption is that, if there is a functional relationship between two molecules, then their abundances should correlate wherever they exist together.

Thus, the co-localization of USO1 with GFP-RAB24, assessed by Pearson's correlation coefficient, is in agreement with a possible functional relationship between USO1 and RAB24. However, the conclusion of a functional relationship would need more experimental support. Firstly, although there was a statistically significant difference in the Pearson's coefficients between the GFP-RAB24 and GFP-expressing cells, the difference was not very large. Secondly, based on the values of the Manders' coefficients, there is only a small degree of overlap between the GFP-RAB24 and USO1 signals. Thirdly, only 15 cells were analyzed in each sample, and the analysis was not repeated (both due to time restrictions). The experiment should be repeated, and more cells should be analyzed to confirm the results.

In summary, the results of this MSc thesis do not allow conclusions on the protein-protein interactions of RAB24 with GOLGA3, USO1 and emerin. More co-IP and co-localization experiments are needed to draw conclusions.

4.3 Conclusions and future perspectives

As described above, there are ways to further optimize the experimental protocols in order to achieve more consistent results and possibly confirm the interaction between RAB24 and the three putative interactors. However, it is also possible that GOLGA3, USO1 and emerin do not physically interact with RAB24. The APEX2 proximity biotinylation assay demonstrated their proximity to RAB24, but this assay does not confirm physical interactions. Indeed, a drawback of the APEX2 method is that the results are 'contaminated' by noninteracting proteins that are localized to the same organelles.

Considering possible follow-up studies, the next step would be to perform repeated co-IPs with the protocol optimization outlined above. Then, if a physical interaction could be established using co-IP, further co-localization analyses with appropriate repetitions and a larger sample size should be performed. In addition, proximity ligation assay could be used to detect co-localization. When functioning optimally, this assay can detect co-localization with high sensitivity and specificity (Alam, 2018).

Overall, it is important to continue investigating RAB24 and its interaction partners to further elucidate the roles RAB24 plays at the late stages of autophagic and endocytic degradation processes, in cell division and cellular energy metabolism. Understanding these molecular processes could help the understating of disease pathogenesis and possibly also provide novel treatment targets for age-related diseases, such as neurodegenerative diseases and cancer (Debnath et al., 2023; Park et al., 2020).

Acknowledgements

Thank you to Eeva-Liisa Eskelinen for providing me with the chance to write this thesis in the Eskelinen group and providing me with valuable guidance and support throughout the whole project. Also, thank you kindly to Lav Tripathi for guiding me in the practical aspects of this project, and deepening my understanding of scientific culture and thinking. I want to thank our group members Mauricio Ramm and Martin Lopez as well, for always answering any of my questions thoroughly. I also want to thank our group members Hira, Yunus, Axel, Farhad, Roosa and Anson, for creating a friendly and collaborative atmosphere.

References

Aaron, J. S., Taylor, A. B., & Chew, T. L. (2018). Image co-localization - Co-occurrence versus correlation. *Journal of Cell Science*, *131*(3). https://doi.org/10.1242/JCS.211847/77151

Agler, C., Nielsen, D. M., Urkasemsin, G., Singleton, A., Tonomura, N., Sigurdsson, S., Tang, R., Linder, K., Arepalli, S., Hernandez, D., Lindblad-Toh, K., van de Leemput, J., Motsinger-Reif, A., O'Brien, D. P., Bell, J., Harris, T., Steinberg, S., & Olby, N. J. (2014). Canine Hereditary Ataxia in Old English Sheepdogs and Gordon Setters Is Associated with a Defect in the Autophagy Gene Encoding RAB24. *PLOS Genetics*, *10*(2), e1003991. https://doi.org/10.1371/JOURNAL.PGEN.1003991

Alam, M. S. (2018). Proximity Ligation Assay (PLA). *Current Protocols in Immunology*, *123*(1), e58. https://doi.org/10.1002/CPIM.58

Alfonso, A., Segev, N., Payne, G. S., & Donaldson, J. (2009). Overview of Intracellular Compartments and Trafficking Pathways [Bookitem]. In *Trafficking Inside Cells*. Springer.

Allan, B. B., Moyer, B. D., & Balch, W. E. (2000). Rab1 recruitment of p115 into a cis-SNARE complex: programming budding COPII vesicles for fusion. *Science (New York, N.Y.)*, *289*(5478), 444–448. https://doi.org/10.1126/SCIENCE.289.5478.444

Alvarez, C., Fujita, H., Hubbard, A., & Sztul, E. (1999). ER to Golgi transport: Requirement for p115 at a pre-Golgi VTC stage. *The Journal of Cell Biology*, *147*(6), 1205–1221. https://doi.org/10.1083/JCB.147.6.1205

Amaya, C., Militello, R. D., Calligaris, S. D., & Colombo, M. I. (2016). Rab24 interacts with the Rab7/Rab interacting lysosomal protein complex to regulate endosomal degradation. *Traffic*, *17*(11), 1181–1196. https://doi.org/10.1111/TRA.12431

Balderhaar, H. J. kleine, & Ungermann, C. (2013). CORVET and HOPS tethering complexes – coordinators of endosome and lysosome fusion. *Journal of Cell Science*, *126*(6), 1307–1316. https://doi.org/10.1242/JCS.107805

Barlowe, C. (1997). Coupled ER to Golgi transport reconstituted with purified cytosolic proteins. *The Journal of Cell Biology*, *139*(5), 1097–1108. https://doi.org/10.1083/JCB.139.5.1097

Barroso, M., Nelson, D. S., & Sztul, E. (1995). Transcytosis-associated protein (TAP)/p115 is a general fusion factor required for binding of vesicles to acceptor membranes. *Proceedings of the National Academy of Sciences*, *92*(2), 527–531. https://doi.org/10.1073/PNAS.92.2.527

Behrends, C., Sowa, M. E., Gygi, S. P., & Harper, J. W. (2010). Network organization of the human autophagy system HHS Public Access. *Nature*, *466*(7302), 68–76. https://doi.org/10.1038/nature09204

Berk, J. M., Tifft, K. E., & Wilson, K. L. (2013). The nuclear envelope LEM-domain protein emerin. *Nucleus*, *4*(4), 298. https://doi.org/10.4161/NUCL.25751

Bione, S., Maestrini, E., Rivella, S., Mancini, M., Regis, S., Romeo, G., & Toniolo, D. (1994). Identification of a novel X-linked gene responsible for Emery-Dreifuss muscular dystrophy. *Nature Genetics 1994 8:4*, *8*(4), 323–327. https://doi.org/10.1038/ng1294-323

Borrego-Pinto, J., Jegou, T., Osorio, D. S., Auradé, F., Gorjánácz, M., Koch, B., Mattaj, I. W., & Gomes, E. R. (2012). Samp1 is a component of TAN lines and is required for nuclear movement. *Journal of Cell Science*, *125*(Pt 5), 1099–1105. https://doi.org/10.1242/JCS.087049

Brandon, E., Szul, T., Alvarez, C., Grabski, R., Benjamin, R., Kawai, R., & Sztul, E. (2006). On and off membrane dynamics of the endoplasmic reticulum-golgi tethering factor p115 in vivo. *Molecular Biology of the Cell*, *17*(7), 2996–3008. https://doi.org/10.1091/MBC.E05-09-0862/ASSET/IMAGES/LARGE/ZMK0070676870007.JPEG

Bui, S., Mejia, I., Díaz, B., & Wang, Y. (2021). Adaptation of the Golgi Apparatus in Cancer Cell Invasion and Metastasis. *Frontiers in Cell and Developmental Biology*, *9*. https://doi.org/10.3389/FCELL.2021.806482

Cao, X., Ballew, N., & Barlowe, C. (1998). Initial docking of ER-derived vesicles requires Uso1p and Ypt1p but is independent of SNARE proteins. *EMBO Journal*, *17*(8), 2156–2165. https://doi.org/10.1093/EMBOJ/17.8.2156

Chang, W., Folker, E. S., Worman, H. J., & Gundersen, G. G. (2013). Emerin organizes actin flow for nuclear movement and centrosome orientation in migrating fibroblasts. *Molecular Biology of the Cell*, *24*(24), 3869. https://doi.org/10.1091/MBC.E13-06-0307

Chavrier, P., Gorvel, J. P., Stelzer, E., Simons, K., Gruenberg, J., & Zerial, M. (1991). Hypervariable C-termmal domain of rab proteins acts as a targeting signal. *Nature 1991 353:6346*, *353*(6346), 769–772. https://doi.org/10.1038/353769a0

Chen, Y., & Li, Y. (2012). *Autophagic lysosome reformation*. https://doi.org/10.1016/j.yexcr.2012.09.004

Chen, Z., Wang, X., Liu, R., Chen, L., Yi, J., Qi, B., Shuang, Z., Liu, M., Li, X., Li, S., & Tang, H. (2017). KDM4B-mediated epigenetic silencing of miRNA-615-5p augments RAB24 to facilitate malignancy of hepatoma cells. *Oncotarget*, *8*(11), 17712. https://doi.org/10.18632/ONCOTARGET.10832

Debnath, J., Gammoh, N., & Ryan, K. M. (2023). Autophagy and autophagy-related pathways in cancer. *Nature Reviews Molecular Cell Biology 2023 24:8*, *24*(8), 560–575. https://doi.org/10.1038/s41580-023-00585-z

Demmerle, J., Koch, A. J., & Holaska, J. M. (2012). The Nuclear Envelope Protein Emerin Binds Directly to Histone Deacetylase 3 (HDAC3) and Activates HDAC3 Activity. *The Journal of Biological Chemistry*, *287*(26), 22080. https://doi.org/10.1074/JBC.M111.325308

Ding, J., Soule, G., Overmeyer, J. H., & Maltese, W. A. (2003). Tyrosine phosphorylation of the Rab24 GTPase in cultured mammalian cells. *Biochemical and Biophysical Research Communications*, *312*, 670–675. https://doi.org/10.1016/j.bbrc.2003.10.171

Dirac-Svejstrup, A. B., Sumizawa, T., & Pfeffer, S. R. (1997). Identification of a GDI displacement factor that releases endosomal Rab GTPases from Rab–GDI. *The EMBO Journal*, *16*(3), 465–472. https://doi.org/10.1093/EMBOJ/16.3.465

Eathiraj, S., Pan, X., Ritacco, C., & Lambright, D. G. (2005). Structural basis of family-wide Rab GTPase recognition by rabenosyn-5. *Nature 2005 436:7049*, *436*(7049), 415–419. https://doi.org/10.1038/nature03798

Egami, Y., Kiryu-Seo, S., Yoshimori, T., & Kiyama, H. (2005). Induced expressions of Rab24 GTPase and LC3 in nerve-injured motor neurons. *Biochemical and Biophysical Research Communications*, *337*(4), 1206–1213. https://doi.org/10.1016/J.BBRC.2005.09.171

Elias, M., Brighouse, A., Gabernet-Castello, C., Field, M. C., & Dacks, J. B. (2012). Sculpting the endomembrane system in deep time: High resolution phylogenetics of Rab GTPases. *Journal of Cell Science*, *125*(10), 2500–2508. https://doi.org/10.1242/JCS.101378/263067/AM/SCULPTING-THE-ENDOMEMBRANE-SYSTEM-IN-DEEP-TIME

Erdman, R. A., Shellenberger, K. E., Overmeyer, J. H., & Maltese, W. A. (2000). *Rab24 Is an Atypical Member of the Rab GTPase Family DEFICIENT GTPase ACTIVITY, GDP DISSOCIATION INHIBITOR INTERACTION, AND PRENYLATION OF Rab24 EXPRESSED IN CULTURED CELLS**. http://www.jbc.org

Evans, I. M., & Paliashvili, K. (2022). Co-immunoprecipitation Assays. *Methods in Molecular Biology*, *2475*, 125–132. https://doi.org/10.1007/978-1-0716-2217-9_8

Folker, E. S., Östlund, C., Luxton, G. W. G., Worman, H. J., & Gundersen, G. G. (2011). Lamin A variants that cause striated muscle disease are defective in anchoring transmembrane actin-associated nuclear lines for nuclear movement. *Proceedings of the National Academy of Sciences of the United States of America*, *108*(1), 131–136. https://doi.org/10.1073/PNAS.1000824108/-/DCSUPPLEMENTAL

Fukuda, M., Kanno, E., Ishibashi, K., & Itoh, T. (2008). Large scale screening for novel rab effectors reveals unexpected broad rab binding specificity. *Molecular and*

Cellular Proteomics, *7*(6), 1031–1042. https://doi.org/10.1074/mcp.M700569-MCP200

Gabe Lee, M. T., Mishra, A., & Lambright, D. G. (2009). Structural Mechanisms for Regulation of Membrane Traffic by Rab GTPases. *Traffic*, *10*(10), 1377–1389. https://doi.org/10.1111/J.1600-0854.2009.00942.X

Gerace, L., & Huber, M. D. (2012). Nuclear lamina at the crossroads of the cytoplasm and nucleus. *Journal of Structural Biology*, *177*(1), 24–31. https://doi.org/10.1016/j.jsb.2011.11.007

Gomes, L. C., Benedetto, G. Di, & Scorrano, L. (2011). During autophagy mitochondria elongate, are spared from degradation and sustain cell viability. *Nature Cell Biology*, *13*(5), 589. https://doi.org/10.1038/NCB2220

Goody, R. S., Rak, A., & Alexandrov, K. (2005). The structural and mechanistic basis for recycling of Rab proteins between membrane compartments. In *Cellular and Molecular Life Sciences* (Vol. 62, Issue 15, pp. 1657–1670). https://doi.org/10.1007/s00018-005-4486-8

Gundersen, G. G., & Worman, H. J. (2013). Nuclear Positioning. *Cell*, *152*(6), 1376. https://doi.org/10.1016/J.CELL.2013.02.031

Haque, F., Mazzeo, D., Patel, J. T., Smallwood, D. T., Ellis, J. A., Shanahan, C. M., & Shackleton, S. (2010). Mammalian SUN Protein Interaction Networks at the Inner Nuclear Membrane and Their Role in Laminopathy Disease Processes. *The Journal of Biological Chemistry*, *285*(5), 3487. https://doi.org/10.1074/JBC.M109.071910

HepG2 Cell Line - A Liver Cancer Research Resource. (n.d.). Retrieved November 11, 2024, from https://www.cytion.com/Knowledge-Hub/Cell-Line-Insights/HepG2-Cell-Line-A-Liver-Cancer-Research-Resource/

Hersheson, J., Haworth, A., & Houlden, H. (2012). The inherited ataxias: Genetic heterogeneity, mutation databases, and future directions in research and clinical diagnostics. *Human Mutation*, *33*(9), 1324–1332. https://doi.org/10.1002/HUMU.22132

Hicks, S. W., Horn, T. A., Mccaffery, J. M., Zuckerman, D. M., & Machamer, C. E. (2006). Golgin-160 promotes cell surface expression of the beta-1 adrenergic receptor. *Traffic*, *7*(12), 1666–1677. https://doi.org/10.1111/J.1600-0854.2006.00504.X

Hicks, S. W., & Machamer, C. E. (2002). The NH2-terminal domain of Golgin-160 contains both Golgi and nuclear targeting information. *The Journal of Biological Chemistry*, *277*(39), 35833–35839. https://doi.org/10.1074/JBC.M206280200

Hicks, S. W., & Machamer, C. E. (2005). Isoform-specific interaction of golgin-160 with the Golgi-associated protein PIST. *Journal of Biological Chemistry*, *280*(32), 28944–28951. https://doi.org/10.1074/jbc.M504937200

Hildebrand, J. D., & Soriano, P. (2002). Overlapping and Unique Roles for C-Terminal Binding Protein 1 (CtBP1) and CtBP2 during Mouse Development. *Molecular and Cellular Biology*, *22*(15), 5296. https://doi.org/10.1128/MCB.22.15.5296-5307.2002

Holaska, J. M., Kowalski, A. K., & Wilson, K. L. (2004). Emerin Caps the Pointed End of Actin Filaments: Evidence for an Actin Cortical Network at the Nuclear Inner Membrane. *PLoS Biology*, *2*(9). https://doi.org/10.1371/JOURNAL.PBIO.0020231

Hong, W. (2005). SNAREs and traffic. *Biochimica et Biophysica Acta (BBA) - Molecular Cell Research*, *1744*(2), 120–144. https://doi.org/10.1016/J.BBAMCR.2005.03.014

Huh-7 Origin - HUH-7 Cell Line. (n.d.). Retrieved September 16, 2024, from https://huh7.com/

Hyttinen, J. M. T., Niittykoski, M., Salminen, A., & Kaarniranta, K. (2013). Maturation of autophagosomes and endosomes: A key role for Rab7 [Article]. *Biochimica et Biophysica Acta. Molecular Cell Research*, *1833*(3), 503–510. https://doi.org/10.1016/j.bbamcr.2012.11.018

Itakura, E., Kishi-Itakura, C., & Mizushima, N. (2012). The hairpin-type tail-anchored SNARE syntaxin 17 targets to autophagosomes for fusion with endosomes/lysosomes. *Cell*, *151*(6), 1256–1269. https://doi.org/10.1016/j.cell.2012.11.001

Itakura, E., & Mizushima, N. (2013). Syntaxin 17: The autophagosomal SNARE. *Autophagy*, *9*(6), 917–919. https://doi.org/10.4161/AUTO.24109/ASSET/DAFD04E0-CEB2-4BAF-A751-CD60145572B5/ASSETS/IMAGES/LARGE/KAUP_A_10924109_F0001.JPG

Jäger, S., Bucci, C., Tanida, I., Ueno, T., Kominami, E., Saftig, P., & Eskelinen, E. L. (2004a). Role for Rab7 in maturation of late autophagic vacuoles. *Journal of Cell Science*, *117*(20), 4837–4848. https://doi.org/10.1242/JCS.01370

Jäger, S., Bucci, C., Tanida, I., Ueno, T., Kominami, E., Saftig, P., & Eskelinen, E.-L. (2004b). Role for Rab7 in maturation of late autophagic vacuoles [Article]. *Journal of Cell Science*, *117*(Pt 20), 4837–4848. https://doi.org/10.1242/jcs.01370

Johnson, D. S., & Chen, Y. H. (2012). *Ras Family of Small GTPases In Immunity And Inflammation*. https://doi.org/10.1016/j.coph.2012.02.003

Kotiniitty, R. (2024). *Rab24:n vuorovaikutus HOPS-kompleksin VPS18:n ja Golgin laitteen GM130:n kanssa*. https://www.utupub.fi/handle/10024/176738

Krishnan, P. D. G., Golden, E., Woodward, E. A., Pavlos, N. J., & Blancafort, P. (2020). Rab GTPases: Emerging Oncogenes and Tumor Suppressive Regulators for the Editing of Survival Pathways in Cancer. *Cancers*, *12*(2). https://doi.org/10.3390/CANCERS12020259

Lee, K. K., Haraguchi, T., Lee, R. S., Koujin, T., Hiraoka, Y., & Wilson, K. L. (2001). Distinct functional domains in emerin bind lamin A and DNA-bridging protein BAF.

Journal of Cell Science, *114*(24), 4567–4573. https://doi.org/10.1242/jcs.114.24.4567

Levine, B., & Kroemer, G. (2008). Autophagy in the Pathogenesis of Disease. *Cell*, *132*(1), 27–42. https://doi.org/10.1016/J.CELL.2007.12.018

Llovet, J. M., Kelley, R. K., Villanueva, A., Singal, A. G., Pikarsky, E., Roayaie, S., Lencioni, R., Koike, K., Zucman-Rossi, J., & Finn, R. S. (2021). Hepatocellular carcinoma. *Nature Reviews. Disease Primers*, *7*(1). https://doi.org/10.1038/S41572-020-00240-3

Luxton, G. W. G., Gomes, E. R., Folker, E. S., Vintinner, E., & Gundersen, G. G. (2010). Linear Arrays of Nuclear Envelope Proteins Harness Retrograde Actin Flow for Nuclear Movement. *Science (New York, N.Y.)*, *329*(5994), 956. https://doi.org/10.1126/SCIENCE.1189072

Margalit, A., Brachner, A., Gotzmann, J., Foisner, R., & Gruenbaum, Y. (2007). Barrier-to-autointegration factor – a BAFfling little protein. *Trends in Cell Biology*, *17*(4), 202–208. https://doi.org/10.1016/J.TCB.2007.02.004

Margalit, A., Segura-Totten, M., Gruenbaum, Y., & Wilson, K. L. (2005). Barrier-to-autointegration factor is required to segregate and enclose chromosomes within the nuclear envelope and assemble the nuclear lamina. *Proceedings of the National Academy of Sciences of the United States of America*, *102*(9), 3290–3295. https://doi.org/10.1073/PNAS.0408364102/SUPPL_FILE/08364FIG7.JPG

Markiewicz, E., Tilgner, K., Barker, N., Van De Wetering, M., Clevers, H., Dorobek, M., Hausmanowa-Petrusewicz, I., Ramaekers, F. C. S., Broers, J. L. V., Blankesteijn, W. M., Salpingidou, G., Wilson, R. G., Ellis, J. A., & Hutchison, C. J. (2006). The inner nuclear membrane protein Emerin regulates β-catenin activity by restricting its accumulation in the nucleus. *EMBO Journal*, *25*(14), 3275–3285. https://doi.org/10.1038/SJ.EMBOJ.7601230/SUPPL_FILE/EMBJ7601230-SUP-0003.DOC

Matsuda, A., Schermelleh, L., Hirano, Y., Haraguchi, T., & Hiraoka, Y. (2018). Accurate and fiducial-marker-free correction for three-dimensional chromatic shift in biological fluorescence microscopy. *Scientific Reports 2018 8:1*, *8*(1), 1–14. https://doi.org/10.1038/s41598-018-25922-7

Matsui, Y., Kikuchi, A., Araki, S., Hata, Y., Kondo, J., Teranishi,' And, Y., & Takai2, Y. (1990). Molecular Cloning and Characterization of a Novel Type of Regulatory Protein (GDI) for smg p25A, a ras p21-Like GTP-Binding Protein. *MOLECULAR AND CELLULAR BIOLOGY*, *10*(8), 4116–4122.

Melcon, G., Kozlov, S., Cutler, D. A., Sullivan, T., Hernandez, L., Zhao, P., Mitchell, S., Nader, G., Bakay, M., & Rottman, J. N. (2006). Lmo7 is an emerin-binding protein that regulates the transcription of emerin and many other muscle-relevant genes.

Human Molecular Genetics, *15*(23), 3459–3472. https://doi.org/10.1093/HMG/DDL423

Milazzo, G., Mercatelli, D., Di Muzio, G., Triboli, L., De Rosa, P., Perini, G., & Giorgi, F. M. (2020). Histone Deacetylases (HDACs): Evolution, Specificity, Role in Transcriptional Complexes, and Pharmacological Actionability. *Genes*, *11*(5). https://doi.org/10.3390/GENES11050556

Militello, R. D., Munafó, D. B., Berón, W., López, L. A., Monier, S., Goud, B., & Colombo, M. I. (2013). Rab24 is Required for Normal Cell Division. *Traffic*, *14*(5), 502–518. https://doi.org/10.1111/tra.12057

Morató, X., Borroto-Escuela, D. O., Fuxe, K., Fernández-Dueñas, V., & Ciruela, F. (2021). Co-Immunoprecipitation from Brain. In *Neuromethods* (Vol. 169, pp. 19–30). Humana Press Inc. https://doi.org/10.1007/978-1-0716-1522-5_2

Munro, S. (2011). The Golgin Coiled-Coil Proteins of the Golgi Apparatus. *Cold Spring Harbor Perspectives in Biology*, *3*(6), 1–14. https://doi.org/10.1101/CSHPERSPECT.A005256

Musiwaro, P., Smith, M., Manifava, M., Walker, S. A., & Ktistakis, N. T. (2013). Characteristics and requirements of basal autophagy in HEK 293 cells. *Autophagy*, *9*(9), 1407–1417. https://doi.org/10.4161/AUTO.25455

Nakajima, H., Hirata, A., Ogawa, Y., Yonehara, T., Yoda, K., & Yamasaki, M. (1991). A cytoskeleton-related gene, uso1, is required for intracellular protein transport in Saccharomyces cerevisiae. *Journal of Cell Biology*, *113*(2), 245–260. https://doi.org/10.1083/JCB.113.2.245

Nakamura, N., Lowe, M., Levine, T. P., Rabouille, C., & Warren, G. (1997). The Vesicle Docking Protein p115 Binds GM130, a cis-Golgi Matrix Protein, in a Mitotically Regulated Manner. *Cell*, *89*(3), 445–455. https://doi.org/10.1016/S0092-8674(00)80225-1

Nastały, P., Purushothaman, D., Marchesi, S., Poli, A., Lendenmann, T., Kidiyoor, G. R., Beznoussenko, G. V., Lavore, S., Romano, O. M., Poulikakos, D., Lagomarsino, M. C., Mironov, A. A., Ferrari, A., & Maiuri, P. (2020). Role of the nuclear membrane protein Emerin in front-rear polarity of the nucleus. *Nature Communications 2020 11:1*, *11*(1), 1–12. https://doi.org/10.1038/s41467-020-15910-9

Nelson, D. S., Alvarez, C., Gao, Y. S., García-Mata, R., Fialkowski, E., & Sztul, E. (1998). The membrane transport factor TAP/p115 cycles between the Golgi and earlier secretory compartments and contains distinct domains required for its localization and function. *The Journal of Cell Biology*, *143*(2), 319–331. https://doi.org/10.1083/JCB.143.2.319

Nguyen, T. M. T., Kim, J., Doan, T. T., Lee, M. W., & Lee, M. (2020). APEX Proximity Labeling as a Versatile Tool for Biological Research. *Biochemistry*, *59*(3), 260–269.

https://doi.org/10.1021/ACS.BIOCHEM.9B00791/ASSET/IMAGES/MEDIUM/BI9B00791_0006.GIF

OLKKONEN, V. M., DUPREE, P., KILLISCH, I., LÜTCKE, A., ZERIAL, M., & SIMONS, K. (1993). Molecular cloning and subcellular localization of three GTP-binding proteins of the rab subfamily [Article]. *Journal of Cell Science*, *106*(4), 1249–1261. https://doi.org/10.1242/jcs.106.4.1249

Park, H., Kang, J. H., & Lee, S. (2020). Autophagy in Neurodegenerative Diseases: A Hunter for Aggregates. *International Journal of Molecular Sciences*, *21*(9). https://doi.org/10.3390/IJMS21093369

Parzych, K. R., & Klionsky, D. J. (2014). An overview of autophagy: morphology, mechanism, and regulation. *Antioxidants & Redox Signaling*, *20*(3), 460–473. https://doi.org/10.1089/ARS.2013.5371

Pereira-Leal, J. B., Hume, A. N., & Seabra, M. C. (2001). Prenylation of Rab GTPases: molecular mechanisms and involvement in genetic disease. *FEBS Letters*, *498*(2–3), 197–200. https://doi.org/10.1016/S0014-5793(01)02483-8

Pylypenko, O., Hammich, H., Yu, I. M., & Houdusse, A. (2018). Rab GTPases and their interacting protein partners: Structural insights into Rab functional diversity. *Small GTPases*, *9*(1–2), 22. https://doi.org/10.1080/21541248.2017.1336191

Qiu, D., Li, S., Guo, L., Yuan, R., & Ou, X. (2019). Rab24 functions in meiotic apparatus assembly and maturational progression in mouse oocyte. *Cell Cycle*, *18*(21), 2893–2901. https://doi.org/10.1080/15384101.2019.1660115

Rensland, H., John, J., Linke, R., Goody, R. S., Simon, I., Schlichting, I., & Wittinghofer, A. (1995). Substrate and Product Structural Requirements for Binding of Nucleotides to H-ras p21: The Mechanism of Discrimination Between Guanosine and Adenosine Nucleotides. *Biochemistry*, *34*(2), 593–599. https://doi.org/10.1021/BI00002A026

Salpingidou, G., Smertenko, A., Hausmanowa-Petrucewicz, I., Hussey, P. J., & Hutchison, C. J. (2007). A novel role for the nuclear membrane protein emerin in association of the centrosome to the outer nuclear membrane. *The Journal of Cell Biology*, *178*(6), 897. https://doi.org/10.1083/JCB.200702026

Sapperstein, S. K., Walter, D. M., Grosvenor, A. R., Heuser, J. E., & Waters, M. G. (1995). p115 is a general vesicular transport factor related to the yeast endoplasmic reticulum to Golgi transport factor Uso1p. *Proceedings of the National Academy of Sciences of the United States of America*, *92*(2), 522–526. https://doi.org/10.1073/PNAS.92.2.522

Schardt, A., Brinkmann, B. G., Mitkovski, M., Sereda, M. W., Werner, H. B., & Nave, K.-A. (2009). The SNARE protein SNAP-29 interacts with the GTPase Rab3A: Implications for membrane trafficking in myelinating glia [Article]. *Journal of Neuroscience Research*, *87*(15), 3465–3479. https://doi.org/10.1002/jnr.22005

Schlager, M. A., Kapitein, L. C., Grigoriev, I., Burzynski, G. M., Wulf, P. S., Keijzer, N., De Graaff, E., Fukuda, M., Shepherd, I. T., Akhmanova, A., & Hoogenraad, C. C. (2010). Pericentrosomal targeting of Rab6 secretory vesicles by Bicaudal-D-related protein 1 (BICDR-1) regulates neuritogenesis. *The EMBO Journal*, *29*(10), 1637. https://doi.org/10.1038/EMBOJ.2010.51

Schneider, A. F. L., & Hackenberger, C. P. R. (2017). Fluorescent labelling in living cells. *Current Opinion in Biotechnology*, *48*, 61–68. https://doi.org/10.1016/J.COPBIO.2017.03.012

Schoebel, S., Oesterlin, L. K., Blankenfeldt, W., Goody, R. S., & Itzen, A. (2009). RabGDI Displacement by DrrA from Legionella Is a Consequence of Its Guanine Nucleotide Exchange Activity. *Molecular Cell*, *36*(6), 1060–1072. https://doi.org/10.1016/J.MOLCEL.2009.11.014

Seidel, K., Siswanto, S., Brunt, E. R. P., Den Dunnen, W., Korf, H. W., & Rüb, U. (2012). Brain pathology of spinocerebellar ataxias. *Acta Neuropathologica 2012 124:1*, *124*(1), 1–21. https://doi.org/10.1007/S00401-012-1000-X

Seitz, S., Kwon, Y., Hartleben, G., Jülg, J., Sekar, R., Krahmer, N., Najafi, B., Loft, A., Gancheva, S., Stemmer, K., Feuchtinger, A., Hrabe de Angelis, M., Müller, T. D., Mann, M., Blüher, M., Roden, M., Berriel Diaz, M., Behrends, C., Gilleron, J., … Zeigerer, A. (2019). Hepatic Rab24 controls blood glucose homeostasis via improving mitochondrial plasticity. *Nature Metabolism*, *1*(10), 1009–1026. https://doi.org/10.1038/s42255-019-0124-x

Seki, Y., Suzuki, S. O., Nakamura, S., & Iwaki, T. (2009). Degenerative and protective reactions of the rat trigeminal motor nucleus after removal of the masseter and temporal muscles. *Journal of Oral Pathology & Medicine*, *38*(10), 777–784. https://doi.org/10.1111/J.1600-0714.2009.00772.X

Settembre, C., Fraldi, A., Medina, D. L., & Ballabio, A. (2013). Signals from the lysosome: a control centre for cellular clearance and energy metabolism. *Nature Reviews Molecular Cell Biology 2013 14:5*, *14*(5), 283–296. https://doi.org/10.1038/nrm3565

Shirane, M., & Nakayama, K. I. (2006). Protrudin induces neurite formation by directional membrane trafficking. *Science*, *314*(5800), 818–821. https://doi.org/10.1126/SCIENCE.1134027

Sinka, R., Gillingham, A. K., Kondylis, V., & Munro, S. (2008). Golgi coiled-coil proteins contain multiple binding sites for Rab family G proteins. *The Journal of Cell Biology*, *183*(4), 607. https://doi.org/10.1083/JCB.200808018

Smirnova, E., Griparic, L., Shurland, D. L., & Van der Bliek, A. M. (2001). Dynamin-related protein Drp1 is required for mitochondrial division in mammalian cells. *Molecular Biology of the Cell*, *12*(8), 2245–2256.

https://doi.org/10.1091/MBC.12.8.2245/ASSET/IMAGES/LARGE/MK0811579008.JPEG

Song, S., Cong, W., Zhou, S., Shi, Y., Dai, W., Zhang, H., Wang, X., He, B., & Zhang, Q. (2019). Small GTPases: Structure, biological function and its interaction with nanoparticles. *Asian Journal of Pharmaceutical Sciences*, *14*, 30–39. https://doi.org/10.1016/j.ajps.2018.06.004

Sönnichsen, B., Lowe, M., Levine, T., Jämsä, E., Dirac-Svejstrup, B., & Warren, G. (1998). A Role for Giantin in Docking COPI Vesicles to Golgi Membranes. *The Journal of Cell Biology*, *140*(5), 1013–1021. http://www.jcb.org

Steegmaier, M., Yang, B., Yoo, J.-S., Huang, B., Shen, M., Yu, S., Luo, Y., & Scheller, R. H. (1998). Three Novel Proteins of the Syntaxin/SNAP-25 Family*. *THE JOURNAL OF BIOLOGICAL CHEMISTRY*, *273*(51), 34171–34179. https://doi.org/10.1074/jbc.273.51.34171

Stenmark, H. (2009). Guanine nucleotide exchange factor A protein that facilitates the exchange of GDP for GTP in the nucleotide-binding pocket of a GTP-binding protein. Rab GTPases as coordinators of vesicle traffic. *NATuRE REvIEwS | Molecular Cell Biology*, *10*, 513. https://doi.org/10.1038/nrm2728

Takahashi, Y. (2015). Co-immunoprecipitation from transfected cells. *Methods in Molecular Biology*, *1278*, 381–389. https://doi.org/10.1007/978-1-4939-2425-7_25

Takáts, S., Nagy, P., Varga, Á., Pircs, K., Kárpáti, M., Varga, K., Kovács, A. L., Hegedűs, K., & Juhász, G. (2013). Autophagosomal Syntaxin17-dependent lysosomal degradation maintains neuronal function in Drosophila [Article]. *The Journal of Cell Biology*, *201*(4), 531–539. https://doi.org/10.1083/jcb.201211160

Tambe, Y., Yamamoto, A., Isono, T., Chano, T., Fukuda, M., & Inoue, H. (2009). The drs tumor suppressor is involved in the maturation process of autophagy induced by low serum. *Cancer Letters*, *283*(1), 74–83. https://doi.org/10.1016/J.CANLET.2009.03.028

Valencia, A., Chardin, P., Wittinghofer, A., & Sander, C. (1991). *Biochemistry © Perspectives in Biochemistry The ras Protein Family: Evolutionary Tree and Role of Conserved Amino Acids*. https://pubs.acs.org/sharingguidelines

Valencia, A., & Sander, C. (1995). The Ras superfamily. *Guidebook to the Sinall GTPases*, 12–19. https://doi.org/10.1093/OSO/9780198599456.003.0002

Vaughan, O. A., Alvarez-Reyes, M., Bridger, J. M., Broers, J. L. V., Ramaekers, F. C. S., Wehnert, M., Morris, G. E., Whitfield, W. G. F., & Hutchison, C. J. (2001). Both emerin and lamin C depend on lamin A for localization at the nuclear envelope. *Journal of Cell Science*, *114*(14), 2577–2590. https://doi.org/10.1242/JCS.114.14.2577

Vetter, I. R., & Wittinghofer, A. (2001). The guanine nucleotide-binding switch in three dimensions. *Science (New York, N.Y.)*, *294*(5545), 1299–1304. https://doi.org/10.1126/SCIENCE.1062023

Wang, H., He, M., Willard, B., & Wu, Q. (2019). Cross-linking, Immunoprecipitation and Proteomic Analysis to Identify Interacting Proteins in Cultured Cells. *Bio-Protocol*, *9*(11). https://doi.org/10.21769/BIOPROTOC.3258

Wang, T., Grabski, R., Sztul, E., & Hay, J. C. (2015a). p115–SNARE Interactions: A Dynamic Cycle of p115 Binding Monomeric SNARE Motifs and Releasing Assembled Bundles. *Traffic*, *16*(2), 148–171. https://doi.org/10.1111/TRA.12242

Wang, T., Grabski, R., Sztul, E., & Hay, J. C. (2015b). p115-SNARE Interactions: A Dynamic Cycle of p115 Binding Monomeric SNARE Motifs and Releasing Assembled Bundles. *Traffic*, *16*(2), 148–171. https://doi.org/10.1111/TRA.12242

Waters, M. G., Clary, D. O., & Rothman, J. E. (1992). A novel 115-kD peripheral membrane protein is required for intercisternal transport in the Golgi stack. *The Journal of Cell Biology*, *118*(5), 1015–1026. https://doi.org/10.1083/JCB.118.5.1015

Wilson, A. L., Erdman, R. A., & Maltese, W. A. (1996). Association of Rab1B with GDP-dissociation Inhibitor (GDI) Is Required for Recycling but Not Initial Membrane Targeting of the Rab Protein. *Journal of Biological Chemistry*, *271*(18), 10932–10940. https://doi.org/10.1074/JBC.271.18.10932

Wu, K. Y., Xie, H., Zhang, Z. L., Li, Z. X., Shi, L., Zhou, W., Zeng, J., Tian, Z., Zhang, Y., Ding, Y. B., & Shen, W. G. (2022). Emerin knockdown induces the migration and invasion of hepatocellular carcinoma cells by up-regulating the cytoplasmic p21. *Neoplasma*, *69*(1), 59–70. https://doi.org/10.4149/NEO_2021_210728N1059

Yadav, S., Puthenveedu, M. A., & Linstedt, A. D. (2012). Golgin160 Recruits the Dynein Motor to Position the Golgi Apparatus. *Developmental Cell*, *23*(1), 153–165. https://doi.org/10.1016/J.DEVCEL.2012.05.023

Yamamoto, A., Cremona, M. L., & Rothman, J. E. (2006). Autophagy-mediated clearance of huntingtin aggregates triggered by the insulin-signaling pathway. *The Journal of Cell Biology*, *172*(5), 719–731. https://doi.org/10.1083/JCB.200510065

Yang, Z., & Klionsky, D. J. (2010). Mammalian autophagy: core molecular machinery and signaling regulation. *Current Opinion in Cell Biology*, *22*(2), 124. https://doi.org/10.1016/J.CEB.2009.11.014

Yin, G., Huang, J., Petela, J., Jiang, H., Zhang, Y., Gong, S., Wu, J., Liu, B., Shi, J., & Gao, Y. (2023). Targeting small GTPases: emerging grasps on previously untamable targets, pioneered by KRAS. *Signal Transduction and Targeted Therapy 2023 8:1*, *8*(1), 1–39. https://doi.org/10.1038/s41392-023-01441-4

Ylä-Anttila, P., & Eskelinen, E. L. (2018). Roles for RAB24 in autophagy and disease. *Small GTPases*, *9*(1–2), 57–65. https://doi.org/10.1080/21541248.2017.1317699

Ylä-Anttila, P., Mikkonen, E., Happonen, K. E., Holland, P., Ueno, T., Simonsen, A., & Eskelinen, E. L. (2015). RAB24 facilitates clearance of autophagic compartments during basal conditions. *Autophagy*, *11*(10), 1833–1848. https://doi.org/10.1080/15548627.2015.1086522

Yoon, S., Choi, J. H., Shah, M., Kwon, S. M., Yang, J., Park, Y. N., Wang, H. J., & Woo, H. G. (2021). USO1 isoforms differentially promote liver cancer progression by dysregulating the ER-Golgi network. *Carcinogenesis*, *42*(9), 1208–1220. https://doi.org/10.1093/CARCIN/BGAB067

Yorimitsu, T., & Klionsky, D. J. (2005). Autophagy: molecular machinery for self-eating. *Cell Death & Differentiation 2005 12:2*, *12*(2), 1542–1552. https://doi.org/10.1038/sj.cdd.4401765

Zhang, Q., Ragnauth, C. D., Skepper, J. N., Worth, N. F., Warren, D. T., Roberts, R. G., Weissberg, P. L., Ellis, J. A., & Shanahan, C. M. (2005). Nesprin-2 is a multi-isomeric protein that binds lamin and emerin at the nuclear envelope and forms a subcellular network in skeletal muscle. *Journal of Cell Science*, *118*(Pt 4), 673–687. https://doi.org/10.1242/JCS.01642

Zhu, G., Liu, J., Terzyan, S., Zhai, P., Li, G., & Zhang, X. C. (2003). High Resolution Crystal Structures of Human Rab5a and Five Mutants with Substitutions in the Catalytically Important Phosphate-binding Loop*. *THE JOURNAL OF BIOLOGICAL CHEMISTRY*, *278*(4), 2452–2460. https://doi.org/10.1074/jbc.M211042200

Appendix

Appendix 1. Solutions

Cell culture medium

MEM Alpha (Biowest, L0476)

10 % FBS (Gibco, 10270-206)

100 μM glycine, L-alanine, L-asparagine, L-aspartic acid, L-glutamic acid,

L-proline and L-serine (MEM Non-Essential Amino Acids Solution 100X, Gibco, 11140050)

2mM glutamine (GlutaMAX, Gibco, 35050061)

Penicillin/Streptomycin (Biowest, L0022)

PBS (pH 7,4)

1,8 mM KH2PO4

10,1 mM Na2HPO4

2,7 mM KCl

137 mM NaCl

Co-immunoprecipitation lysis buffer

150mM NaCl

1% NP-40

50mM tris-Cl (pH 7.4)

0,5% Sodium deoxycholate (DOC)

EDTA-free protease inhibitor tablet (Thermo Scientific, A32955)

Phosphatase inhibitor tablet (Thermo Scientific, A32957)

1,25 ul of Benzonase (approx. 400U/ul) per ml of buffer. i.e, final conc. is 500U/ml

1mM MgCl2

Co-immunoprecipitation wash buffer

150mM NaCl

1% NP-40

50mM tris-Cl (pH 7.4)

0,5% Sodium deoxycholate (DOC)

1,25 ul of Benzonase (approx. 400U/ul) per ml of buffer. i.e, final conc. is 500U/ml

1mM MgCl2

4X Laemmli buffer

8 % SDS

0,2 M Tris-HCl (pH 6,8)

48 % glycerol

2 % mercaptoethanol

0,02 % bromophenol

Running buffer

192 mM glycine

0,1 % SDS

25 mM Tris

Transfer buffer

192 mM glycine

20 % methanol

25 mM Tris

TBST (pH 7,6)

20 mM Tris-HCl

0,1 % Tween-20

150 mM NaCl

Stripping buffer

1 g SDS

10 mL Tween 20

15 g glycine

Dissolve in 800 mL distilled water

Adjust pH to 2,2

Bring volume up to 1 L with distilled water

Mowiol mounting solution

12 ml 0,2 M Tris (pH 8,5)

2,5 % DAPCO (1,4-diazabicyclo- [2,2,2]-octane; Sigma-Aldrich, D2522)

1 µg/ml DAPI (4',6-diamidino-2-fenyyli-indoli; ThermoFisher Scientific, 62247)

2,4 g Mowiol 4-88 (Sigma-Aldrich, 81381)

6 g glycerol

6 ml MQ-water

Appendix 2. pEGFP-C1 plasmid used in the transient transfections

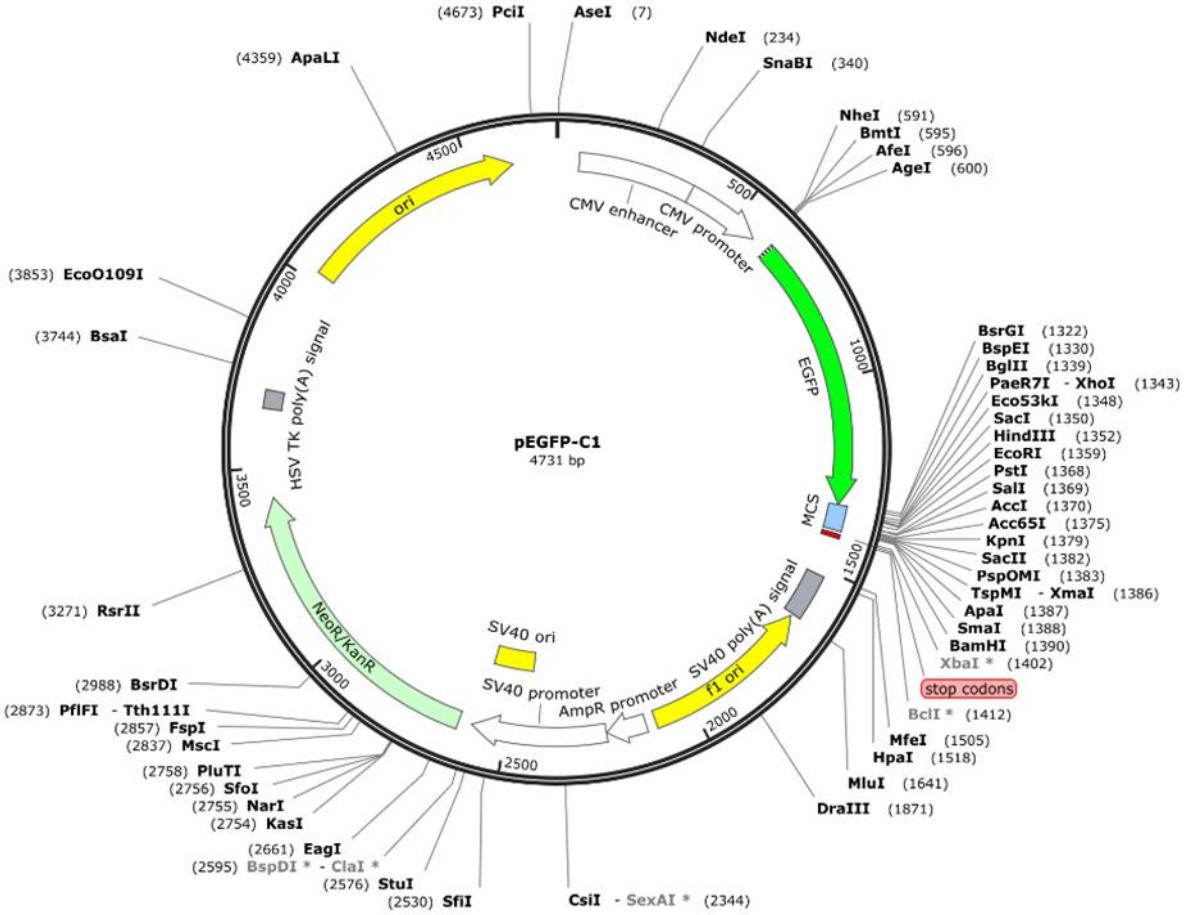

Appendix 3. Nucleobond® Midiprep protocol

Plasmid DNA purification (NucleoBond® Xtra Midi / Maxi)

Protocol at a glance (Rev. 16)

	Midi		Maxi	
1–3 Cultivation and harvest	4,500–6,000 x *g* 4 °C, 15 min			
4–5 Cell lysis *(Important: Check Buffer LYS for precipitated SDS)*	High-copy / low-copy 8 mL / 16 mL Buffer RES 8 mL / 16 mL Buffer LYS RT, 5 min		High-copy / low-copy 12 mL / 24 mL Buffer RES 12 mL / 24 mL Buffer LYS RT, 5 min	
6 Equilibration of the column and filter	12 mL Buffer EQU		25 mL Buffer EQU	
7 Neutralization	8 mL / 16 mL Buffer NEU Mix thoroughly until colorless		12 mL / 24 mL Buffer NEU Mix thoroughly until colorless	
8 Clarification and loading of the lysate	Invert the tube 3 times Load lysate on NucleoBond® Xtra Column Filter			
9 1st Wash	5 mL **Buffer EQU** !		15 mL **Buffer EQU** !	
10 Filter removal	Discard NucleoBond® Xtra Column Filter		Discard NucleoBond® Xtra Column Filter	
11 2nd Wash	8 mL **Buffer WASH** !		25 mL **Buffer WASH** !	
12 Elution	5 mL Buffer ELU		15 mL Buffer ELU	
13 Precipitation	**NucleoBond® Xtra Midi**	**NucleoBond® Xtra Midi Plus**	**NucleoBond® Xtra Maxi**	**NucleoBond® Xtra Maxi Plus**
	3.5 mL Isopropanol Vortex 4,5–15,000 x *g* 4 °C, 30 min	3.5 mL Isopropanol Vortex RT, 2 min Load NucleoBond® Finalizer	10.5 mL Isopropanol Vortex 4,5–15,000 x *g* 4 °C, 30 min	10.5 mL Isopropanol Vortex RT, 2 min Load NucleoBond® Finalizer Large
14 Washing and drying	2 mL 70 % ethanol 4,5–15,000 x *g* RT, 5 min 10–15 min	2 mL 70 % ethanol ≥ 6 x air until dry	4 mL 70 % ethanol 4,5–15,000 x *g* RT, 5 min 15–30 min	4 mL 70 % ethanol ≥ 6 x air until dry
15 Reconstitution	Appropriate volume of TE buffer	200–800 µL Buffer TRIS	Appropriate volume of TE buffer	400–1000 µL Buffer TRIS

MACHEREY-NAGEL GmbH & Co. KG · Neumann-Neander-Str. 6–8 · 52355 Düren · Germany
Tel.: +49 24 21 969-270 · tech-bio@mn-net.com · ***www.mn-net.com***

Appendix 4. jetOPTIMUS® DNA Transfection protocol

jetOPTIMUS® transfection reagent

Short protocol – DNA transfection

DNA TRANSFECTION

Day 0: Cell seeding

→ Seed cells in V mL of cell growth medium according to the table below

Quantities per well, dish or flask

Culture vessel	Number of cells*	V = volume of medium during transfection
96-well	7500 - 25 000	0.125 mL
24-well	40 000 - 100 000	0.5 mL
12-well	80 000 - 200 000	1 mL
6-well / 35 mm	150 000 - 400 000	2 mL
60 mm / flask 25 cm^2	200 000 - 850 000	5 mL
100 mm / flask 75 cm^2	1 x 10^6 - 4 x 10^6	10 mL

*For specific cell type or suspension cells, please refer to the complete protocol.

Day 1: Transfection using jetOPTIMUS® reagent

→ Use jetOPTMUS® buffer only

→ Transfect cells at 60-80% confluency

Dilute X µg of DNA in W µL of jetOPTIMUS® buffer. Vortex 1 s and spin down

Add Y µL of jetOPTIMUS® reagent (starting ratio 1:1)

Vortex 1 s, spin down and incubate 10 min at RT

Add transfection mix to the cells

Incubate 24 to 48 h

Quantities per well, dish or flask

Culture vessel	W = volume of jetOPTIMUS® buffer	X = amount of DNA added	Y = volume of jetOPTIMUS® reagent
96-well	12.5 µL	0.13 µg	0.13 – 0.19 µL
24-well	50 µL	0.5 µg	0.5 – 0.75 µL
12-well	100 µl	1 µg	1 – 1.5 µL
6-well / 35 mm	200 µL	2 µg	2 – 3 µL
60 mm / flask 25 cm^2	500 µL	4 µg	4 – 6 µL
100 mm / flask 75 cm^2	1000 µL	10 µg	10 – 15 µL

Day 2-3: Measure gene expression

See back page for optimization tips

Download complete protocol on https://myaccount.polyplus-transfection.com/

+33 (0)3 90 40 61 80
support@polyplus-transfection.com
www.polyplus-transfection.com

Polyplus